HHS Public Access

Author manuscript

Nat Plants. Author manuscript; available in PMC 2020 October 13.

Published in final edited form as:

Nat Plants. 2020 April ; 6(4): 416–426. doi:10.1038/s41477-020-0634-2.

A mobile ELF4 delivers circadian temperature information from shoots to roots

Wei Wei Chen[1,*], **Nozomu Takahashi**[1,*], **Yoshito Hirata**[2,3], **James Ronald**[4], **Silvana Porco**[5], **Seth J. Davis**[4,6], **Dmitri A. Nusinow**[7], **Steve A. Kay**[5,8], **Paloma Mas**[1,9,†]

[1]Centre for Research in Agricultural Genomics (CRAG), CSIC-IRTA-UAB-UB, Campus UAB, Bellaterra, 08193 Barcelona, Spain.

[2]Mathematics and Informatics Center, The University of Tokyo, 7-3-1 Hongo, Bunkyo-ku, Tokyo 113-8656, Japan.

[3]Faculty of Engineering, Information and Systems, University of Tsukuba, 1-1-1 Tennodai, Tsukuba, Ibaraki 305-8573, Japan.

[4]Department of Biology, University of York, York, UK.

[5]Keck School of Medicine, University of Southern California, Los Angeles, California 90089, United States.

[6]Key Laboratory of Plant Stress Biology, School of Life Sciences, Henan University, Kaifeng 475004, China.

[7]Donald Danforth Plant Science Center, St. Louis, MO 63132.

[8]Institute of Transformative Bio-Molecules, Nagoya University, Nagoya 464-8601, Japan.

[9]Consejo Superior de Investigaciones Científicas (CSIC), 08028 Barcelona, Spain.

Abstract

The circadian clock is synchronized by environmental cues, mostly by light and temperature. Elucidating how the plant circadian clock responds to temperature oscillations is crucial to understand plant responsiveness to the environment. Here we found a prevalent temperature-dependent function of the Arabidopsis clock component ELF4 (EARLY FLOWERING 4) in the root clock. Although the root clock is able to run in the absence of shoots, micrografting assays and mathematical analyses show that ELF4 moves from shoots to regulate rhythms in roots. ELF4 movement does not convey photoperiodic information but trafficking is essential to control the period of the root clock in a temperature-dependent manner. At low temperatures, ELF4 mobility

†Correspondence to: paloma.mas@cragenomica.es.
*These authors contributed equally the manuscript.

Author Contributions

W.W.C, N.T. and J.R. performed the biological experiments. Y.H. performed the mathematical analysis. S.P., S.J.D., D.A.N. and S.A.K. contributed with reagents and comments. P.M. designed the experiments and wrote the manuscript. All authors read, revised, and approved the manuscript.

Competing interests

The authors declare no competing interests.

is favored, resulting in a slow-paced root clock while high temperatures decrease movement, leading to a faster clock. Hence, the mobile ELF4 delivers temperature information and establishes a shoot-to-root dialogue that sets the pace of the clock in roots.

Introduction

Nearly all photosensitive organisms have evolved timing mechanisms or circadian clocks able to synchronize metabolism, physiology and development in anticipation to the 24-hour light/dark cycles[1]. In *Arabidopsis thaliana*, the molecular clockwork is based on complex regulatory networks of core clock components that generate rhythms in a myriad of biological outputs[2, 3]. Appropriate phasing of biological processes relies on clock resetting by light and temperature cues; a mechanism that requires effective changes in the expression and activity of essential clock components[4]. Circadian clocks are also defined by a conserved feature known as temperature compensation[5]. In contrast to the temperature dependency of many physicochemical and biological activities, the circadian clock is able to maintain a constant period over a range of physiological temperatures. By virtue of different transcriptional, post-transcriptional and post-translational mechanisms[6–9], the plant circadian system buffers the circadian period length. Therefore, the circadian clock is able to sustain a period close to 24-hours within a physiological range of temperatures. An ample collection of light-related factors[10–14] and clock-associated components[9, 15, 16] has been shown to directly or indirectly regulate clock temperature compensation in plants.

Among the Arabidopsis clock components, ELF4 (EARLY FLOWERING 4) was initially identified by its role in photoperiod perception and circadian regulation[17]. Structural and functional studies provided a view of the multiple entry points of ELF4 function within the clock[18]. ELF4 protein assembles into a tripartite complex (Evening Complex, EC) together with ELF3 and LUX ARRHYTHMO or PHYTOCLOCK1 (LUX/PCL1)[19, 20]. The complex regulates growth and represses circadian gene expression[21, 22]. ELF4 promotes the nuclear localization of ELF3[19] while LUX directly binds to the promoters of the target genes and thus facilitates the recruitment of ELF4 and ELF3[20, 23]. Loss-of-function mutants of any of the EC components lead to arrhythmia[17, 24–26]. Through multiple interactions with light, clock and photomorphogenesis related factors[27], the EC is able to coordinate plant responses to environmental cues including temperature[15, 27–31] although ELF4, ELF3 and LUX also display independent functions from the EC[31–33].

Regarding the circadian structure and organization within the plant, it is broadly accepted that every plant cell harbors a circadian oscillator. However, circadian communication or coupling among cells and tissues varies at different parts of the plant[34–38]. For instance, while cotyledon cells present circadian autonomy[39], different degrees of cell-to-cell coupling have been reported in leaves[40–42], in the vasculature with neighbor mesophyll cells[43], in guard cells[44], in cells at the root tip[45, 46] and within the shoot apex[47]. Long-distance shoot-to-root photosynthetic signaling is also important for clock entrainment in roots[48] and light piping down the root[49] contributes to this entrainment. Micrografting assays and shoot excision[47] suggest the existence of a long-distance mobile circadian signal

from shoots to roots. Here we report that ELF4 moves from shoots to control the pace of the root clock in a temperature-dependent manner.

Results

Prevalent function of ELF4 sustaining rhythms in roots

We first approached the investigation of the circadian mobile signal by simultaneously following rhythms in shoots and roots of intact plants[47]. The waveforms of the morning-expressed *CCA1* (*CIRCADIAN CLOCK ASSOCIATED 1*) and *LHY* (*LATE ELONGATED HYPOCOTYL*) promoter activities displayed a long period, slightly reduced amplitude and phase delay in roots (Rt) compared to shoots (Sh) (Fig. 1a–b and Extended Data Fig. 1a). The mRNA rhythmic accumulation assayed by Reverse Transcription-Quantitative Polymerase Chain Reaction (RT-QPCR) followed the same trend (Fig. 1c). Similar patterns were observed for the promoter activity of the evening-expressed clock component *TOC1/PRR1* (*TIMING OF CAB EXPRESSION1/PSEUDO RESPONSE REGULATOR1*) (Extended Data Fig. 1b–c). Therefore, the clock is fully operative in roots but its overall pace is slower and the phase delayed compared to shoots.

Under free-running conditions, the circadian clock is unable to properly run in mutant plants of any of the EC components[17, 24–26]. We therefore examined the role of the EC components in the root clock, and in particular, we focused on ELF4. Circadian time course analyses showed that although some very weak oscillations could be appreciated (Extended Data Fig. 1d), the *CCA1* and *LHY* promoter activities and mRNA expression was suppressed in *elf4–1* mutant compared to WT roots (Fig. 1d and Extended Data Fig. 1e–g) following a similar trend to that described in shoots[22] (Extended Data Fig. 1h–j). Over-expression of ELF4 (ELF4-ox) lengthened the period of *LHY::LUC* (Fig. 1e and Extended Data Fig. 1k) indicating that increased ELF4 activity in roots makes the clock to run slow. The expression of *PRR9 (PSEUDO-RESPONSE REGULATOR 9)*, a previously described direct target of the EC in shoots, was clearly up-regulated in *elf4–1* mutant roots (Fig. 1f) suggesting that the EC also represses *PRR9* in roots. Thus, ELF4 plays an important regulatory function in the root clock: mutation compromises rhythms while over-expression lengthens the circadian period.

RNA-Seq analyses of WT and *elf4–1* mutant roots provided a genome-wide view of ELF4 function in roots (Supplementary Table 1). We found that about 15% of the root genes were significantly mis-regulated by the absence of a functional ELF4, with a similar proportion of up-regulated (1297) and down-regulated (1555) genes (Fig. 1g–h and Extended Data Fig. 2a). The expression of core clock genes was amongst the most significantly mis-regulated (Fig. 1i, Extended Data Fig. 2b–i) with a significant fraction of the mis-regulated genes being controlled by the clock, with phase enrichments during the subjective morning and subjective midday (Fig. 1j–k). Functional analyses showed that in addition to the enrichment of genes related to the circadian system and rhythmic processes, genes mis-expressed in *elf4–1* mutant were ascribed to several functional categories including among others responses to stimuli (Supplementary Table 1). Consistently, mis-expression of ELF4 affected physiological outputs such as the number of lateral roots (Extended Data Fig. 2j). Together, the results indicate a prevalent function for ELF4 sustaining rhythms in roots.

ELF4 moves from shoots to regulate oscillator gene expression in roots

Our previous study showed that a signal from shoots is important for circadian rhythms in roots[47]. Micrografting assays are a powerful tool to identify the nature of mobile signals. The grafting technique *per se* does not alter the rhythms in roots[47], as grafted WT scions into WT roots show similar rhythms as non-grafted WT plants (Extended Data Fig. 3a and b). By micrografting different genotypes, we found that grafts of ELF4-ox shoots into *elf4–1* rootstocks [ELF4-ox(Sh)/*elf4–1*(Rt)] (Extended Data Fig. 3c) were particularly efficient in recovering the rhythms in roots (Fig. 2a and Extended Data Fig. 3d). The results are noteworthy as *CCA1::LUC* rhythms are affected in *elf4–1* mutant roots (Fig. 1d). Restoration of the rhythms was reflecting the circadian function exclusively in roots as water instead of luciferin was applied to shoots (ELF4-ox, Sh, H_2O) to avoid luminescence signals leaking from shoots into roots of adjacent wells. Rhythms in roots were also recovered when ELF4-ox scion was grafted into *elf4–2* mutant (Extended Data Fig. 3e) rootstocks (Fig. 2b). To exclude the possibility that the observed results were due to the high over-expression of ELF4-ox plants, we grafted WT shoots into *elf4–1* roots. Although the recovery of the rhythms was not as robust as with ELF4-ox grafts, a rhythmic pattern was observed in roots (Fig. 2c). Thus, ELF4 mRNA or protein are able to move from shoots to roots. This notion was reinforced by the results showing the rhythmic recovery of *elf4–1* rootstocks grafted with ELF4 Minigene (E4MG) scion (Fig. 2d and Extended Data Fig. 3f). These results rule out the possibility that the recovery of the rhythms was just due to the high over-expression of ELF4-ox scion. The influence of shoots as a driving rhythmic force of *elf4–1* rootstocks was also mathematically analyzed with recurrence plots obtained by delay coordinates of the grafting time series. The waveforms of the driving rhythmic force reconstructed from the driven system and their autocorrelation analyses showed a strong periodicity after grafting (Extended Data Fig. 4a–h). In analyses with 10000 randomly shuffled surrogates using as null hypothesis of no serial dependence, we obtained before grafting a p-value of 0.2341 (black dash line) (Extended Data Fig. 4f) and 0.0004 (gray dash line) after grafting (Extended Data Fig. 4h). The statistics are therefore consistent with the notion that rhythms in roots are being forced by a signal from shoots.

To investigate whether the mRNA could be the mobile signal, we performed RT-QPCR time course analyses of roots from ELF4-ox (Sh)/*elf4–1*(Rt) grafts. Our results showed no detectable amplification of *ELF4* mRNA at any time point analyzed (Fig. 2e), which suggest that *ELF4* mRNA did not move through the graft junctions. To confirm this notion, we injected purified ELF4 protein into *elf4–1* mutant (Extended Data Fig. 5a–c). Injection in shoots was able to restore rhythms in roots (Fig. 2f). The percentage of ELF4-injected plants with recovered rhythms was low (5–8%) but was reproducibly observed in different biological replicates. The fact that rhythms were actually restored (Relative Amplitude Errors, RAE<0.6) is supportive of a mobile ELF4 protein from shoots to roots. Rhythmic recovery was not apparent when purified GFP (GREEN FLUORESCENT PROTEIN) was injected (Fig. 2f). The movement of ELF4 protein was further assayed by using shoots of plants over-expressing ELF4 fused to GFP grafted into *elf4–1* mutant roots. Confocal imaging showed that ELF4-GFP fluorescent signals accumulated in the vasculature of *elf4–1* mutant rootstock, across the graft junctions (Fig. 2g–h and Extended Data Fig. 5d–e). Furthermore, Western-blot analyses of roots from ELF4-GFP (Sh)/*elf4–1*(Rt) micrografts

showed that ELF4 protein was effectively detected as a band of the expected size (arrows in Fig. 2i) not present in protein extracts of *elf4–1* mutant roots (Fig. 2i). Grafting ELF4-ox fused to three GFPs (ELF4-x3GFP) scion into *elf4–2* mutant rootstock did not lead to an obvious recovery of rhythms (Fig. 2j and Extended Data Fig. 5f) suggesting the requirement of a mobile ELF4 protein. The ELF4-x3GFP is still functional as its over-expression in the *elf4–1* mutant background restored the hypocotyl phenotypes of *elf4–1* mutant (Extended Data Fig. 5g) and repressed *PRR9* gene expression (Extended Data Fig. 5h–i). The functional relevance of ELF4 movement was also verified in *elf4–1*(Sh)/*elf4–1*(Rt) grafts showing the lack of rhythmic recovery in *elf4–1* roots when *elf4–1* was used as scion (Extended Data Fig. 5j–k). Therefore, multiple series of evidence including the ELF4 injection data, the grafting assays showing the recovery of the rhythms, the ELF4-GFP fluorescent signals across the graft junctions, the detection of the ELF4 protein in roots of the grafted plants, the lack of rhythmic recovery in roots of ELF4-x3GFP and in *elf4–1* scion grafts, support the notion that ELF4 protein moves from shoots to regulate rhythms in roots. Other mobile proteins such as FT (FLOWERING LOCUS T), and HY5 (LONG HYPOCOTYL 5) share some features with ELF4 protein in terms of low molecular weight and high isoelectric point (Fig. 2k).

Blocking ELF4 movement by shoot excision alters circadian rhythms in roots

We next attempted to unveil the function of the mobile ELF4 by blocking ELF4 movement through shoot excision. Analyses of the rhythms showed that excised roots sustained robust oscillations (Extended Data Fig. 6a–b) confirming that the root clock is able to run in the absence of shoots. However, comparison of intact versus excised roots uncovered a shorter period in excised roots (Extended Data Fig. 6c–d). As accumulation of ELF4 results in long periods in shoots[22] and roots (Fig. 1e and Extended Data Fig. 1k), it is plausible that blocking ELF4 movement by shoot excision leads to shorter periods in excised roots. If that is the case, blocking ELF4 movement should also affect ELF4 target gene expression in excised roots. Time course analyses by RT-QPCR revealed that the expression of *PRR9* and *PRR7* was up-regulated in excised roots compared to intact roots (Extended Data Fig. 6e–f), which suggest that in the absence of ELF4 movement from shoots, repression of these genes is alleviated in roots. The use of ELF4-ox intact roots confirmed that *PRR9* and *PRR7* are targets of ELF4 as their expression was clearly down-regulated in intact ELF4-ox roots compared to WT intact roots (Extended Data Fig. 6g–h). Furthermore, ELF4-ox excised roots still showed repression of target gene expression (Extended Data Fig. 6i–j) suggesting that excision *per se* is not responsible for the up-regulation observed in WT excised roots.

To further uncover the function of ELF4 movement, we performed RNA-Seq analyses of WT intact versus excised roots. Our results showed that as expected, a significant fraction of genes was affected by excision (Suplementary Table 2). Comparative analyses of *elf4–1* intact roots with WT excised roots allowed us to discern the effects due to excision from those due to the lack of ELF4 movement (Extended Data Fig. 7). Indeed, we focused on the differentially expressed genes (DEGs) present in both excised WT and intact *elf4–1* roots. As *elf4–1* mutant roots are intact, the overlapping DEGs are not affected by excision *per se* but rather by the lack of ELF4 movement from shoots, which is shared by *elf4–1* intact roots and WT excised roots. Our comparative analyses of both datasets revealed that 67% of the

DEGs in *elf4–1* intact roots are also differentially expressed in WT excised roots (Suplementary Table 3) (Extended Data Fig. 7). The proportion of overlapped DEGs (67%) is highly significant (P-value < 0.0001, chi-square test for equality of proportions) as compared to the proportion of overlapping genes (26%) using a random gene list. The overlap is noteworthy due to the different genotypes (*elf4–1* mutant versus WT) and most importantly, the different conditions (intact versus excised). As WT excised roots and *elf4–1* intact roots share the lack of ELF4 movement from shoots, the overlapping DEGs provides a hint about genes that directly or indirectly require ELF4 movement for proper expression in roots. Consistently, the overlap of DEGs included nearly all of the core oscillator genes (Suplementary Table 3 and Extended Data Fig. 6k). A significant fraction of overlapped DEGs also circadianly oscillated with phase enrichments during the subjective morning and subjective midday (Extended Data Fig. 6l). Therefore, ELF4 movement appears to be important for a fully functional clock in roots.

Mobile ELF4 does not regulate the photoperiodic-dependent phase in roots

In aerial tissues, the circadian clock controls the photoperiodic regulation of growth and development[50]. To determine whether ELF4 movement is important to deliver photoperiodic information, we analyzed rhythms under short day (ShD) and long day (LgD) conditions. In roots, *PRR9::LUC* waveforms displayed a subtle phase delay under LgD compared to ShD (Fig. 3a) following a similar trend to that observed in shoots (Fig. 3b). Time course analyses by Western-blot of roots of ELF4 Minigene plants[20] confirmed the phase delay of ELF4 protein accumulation under LgD compared to ShD (Fig. 3c–d). We reasoned that if ELF4 movement is correlated with the photoperiodic-dependent phase delay, then excision of shoots might affect the phase shift in roots. In agreement with the oscillations in promoter activity (Extended Data Fig. 6c–d), the phase of ELF4 protein accumulation was advanced following excision under both LgD and ShD (Extended Data Fig. 8a–d). Interestingly, under LgD conditions, excision rendered a similar pattern of ELF4 accumulation than in intact roots under ShD (Fig. 3e–f). Therefore, excision abolished the phase delay observed in intact root under LgD (compare Fig. 3c–d with Fig. 3e–f). The results suggest that the photoperiodic-dependent phase shift in roots is hampered by blocking ELF4 movement. However, excised roots still showed the phase delay under LgD compared to excised roots under ShD (Extended Data Fig. 8e–f). Furthermore, analyses of rhythms under LgD conditions showed that plants mis-expressing ELF4 (ELF4-ox and *elf4–1* mutant) displayed very similar rhythms to WT both in shoots and roots (Fig. 3g–h) suggesting that ELF4 function is not essential to sustain rhythms under entraining conditions. Together, the results suggest that blocking ELF4 movement by excision advances the phase of the root clock but the mobile ELF4 does not directly regulate the photoperiodic-dependent phase shift in roots.

ELF4 movement contributes to the temperature-dependent changes in circadian period of the root clock

As the EC also coordinates temperature responses, we examined whether a mobile ELF4 can convey temperature information from shoots to roots. To that end, we first examined the effect of different temperatures (28°C, 18°C and 12°C) on circadian rhythms in roots. We found that *LHY::LUC* circadian period length was shorter at high than at low temperatures (Extended Data Fig. 9a–b). Shortening of period length at increasing temperature was also

observed for other circadian reporter lines (Extended Data Fig. 9c–f) indicating that at this developmental stage and under our experimental conditions, the circadian clock in roots is not able to perfectly sustain circadian period length within a range of temperatures.

As ELF4 accumulation lengthens period length, we next examined the possible contribution of ELF4 to the long period phenotype at low temperatures. Changes in period length could be mediated by increased ELF4 activity and/or by the increased protein movement from shoots to roots. To examine these possibilities, we compared the effects of blocking ELF4 movement by excision at low and high temperatures. Essentially, if the long period in roots at 12°C is independent of movement but results from the increased activity of ELF4, blocking movement from shoots by excision should not have a major effect on period length. However, if ELF4 movement contributes to the period regulation, abolishing ELF4 traffic should lead to an observable and differential effect on period length at different temperatures.

Our results showed that excision shortened the period length in WT roots and this effect was significant at 12°C as compared to the minor effect at 28°C (Extended Data Fig. 10a–d). Therefore, blocking ELF4 movement by excision shortens the long period of WT roots at 12°C. Analyses of other circadian reporter lines and at 18°C also showed that excision shortened period length compared to intact roots (Extended Data Fig. 10e–f). The results suggest a temperature-dependent control of ELF4 movement that regulates period length in roots. To further verify this notion, we examined rhythmic recovery in grafts of ELF4-ox scion into *elf4–1* rootstock at low and high temperatures. Our results showed an evident rhythmic recovery at 12°C but not at 28°C (Fig. 4a–b). Furthermore, grafts of E4MG scion into *elf4–1* rootstock also efficiently recovered rhythms at 12°C but not at 28°C (Fig. 4c–d). ELF4 is still able to delay the phase and lengthen the period at 28°C (Fig. 4e and Extended Data Fig. 10g) suggesting that movement rather than changes in activity are responsible for the observed effects. ELF4 protein accumulation in roots of ELF4-ox scion into *elf4–1* rootstock was higher at 12°C than at 28°C (Figure 4f and Extended Data Fig. 10h–i) but ELF4 (E4MG) protein accumulation in shoots is similar at different temperatures[31] (Extended Data Fig. 10j). Therefore, ELF4 movement rather than protein accumulation or activity appears to be regulated by temperature, contributing to the temperature-dependent control of circadian period in roots.

Altogether, we propose a model by which mobile ELF4 (mbE4) from shoots to roots defines a pool of active ELF4 protein that is competent to repress target circadian gene expression in roots. ELF4 trafficking is favored at low temperatures, which results in a slow-paced clock (Fig. 4g) while high temperatures decrease the movement, leading to a fast root clock (Fig. 4h). The temperature-dependent movement of ELF4 allows a shoot-to-root dialogue that controls the pace of the clock and provides a mechanism by which temperature cues from shoots set the circadian period length in roots.

Discussion

The simultaneous examination of rhythms in shoots and roots of single individual plants shows that the promoter activities and mRNA accumulation of clock genes in roots display a

longer period and delayed phase compared to shoots. The trend was observed for morning- and evening-expressed key oscillator genes suggesting that the overall circadian system in roots is not as precise as in other parts of the plant (e.g. the shoot apex)[47]. Despite the long period, the rhythms persist in roots for several days under LL, which is reminiscent of a fully functional clock. The lack of precision might provide circadian flexibility for rapid adjustments and improved responses in roots. Previous studies have reported spatial waves of clock gene expression with and within organs[40, 42, 45] that might be due to differences in period length and variable local coupling.

The EC directly represses *PRR9* and *PRR7* expression[19, 23, 29, 51, 52] and indirectly promotes the expression of the morning-expressed oscillator genes *CCA1* and *LHY*[51–54]. Our analyses with *elf4–1* mutant and ELF4-ox plants demonstrate that ELF4 function in roots is also important for proper repression of *PRR9* and *PRR7* and activation of *CCA1* and *LHY*. ELF4 regulatory function in roots appears to be similar to that previously described for the EC using whole plants. Over-expression of ELF4 lengthens the period of the root clock suggesting that ELF4 slows down the circadian period in roots as in shoots[22]. The fact that accumulation of ELF4 lengthens the period agrees with the results showing that blocking movement by shoot excision shortens the period. RNA-Seq analyses revealed that not only the expression of oscillator genes is affected in *elf4–1* roots but also a battery of genes involved in other pathways including responses to stimuli. These pathways are also consistent with the EC function in responses to environmental cues[55]. The mis-regulated genes in *elf4–1* roots might be direct targets of ELF4 and/or indirect outputs of the clock in roots. One of these outputs might be lateral root emergence as the number of lateral roots is affected in *elf4–1* and ELF4-ox compared to WT. Future studies are necessary to uncover the molecular and cellular mechanisms by which ELF4 regulates the number of lateral roots in Arabidopsis.

Micrografts of ELF4-ox scion into *elf4–1* or *elf4–2* rootstocks allow a remarkable recovery of rhythms that is not observed when seedlings expressing ELF4 protein fused to 3 GFPs in tandem is used as scion. These results suggest that ELF4 movement is indeed important for the rhythmic recovery. Fluorescent signals accumulating in the vasculature of *elf4–1* mutant rootstock grafted with ELF4-GFP scion and the detection of the ELF4 protein in roots of the micrografted plants also suggest that ELF4 moves from shoots to roots. This conclusion is complemented with the grafting assays of *elf4–1*(Sh)/*elf4–1*(Rt) showing the lack of rhythmic recovery in roots, and with the assays of ELF4 protein injection in shoots and the subsequent rhythmic recovery in roots. Micrografts of E4MG and WT plants are also able to recover the rhythms of the *elf4–1* mutant roots, which indicate that the effects are not due to the over-accumulation of ELF4-ox and suggest that the amount of mobile ELF4 that is required to regulate the rhythms is probably not very high. Our experiments adding water to the scion or using WT scion without LUC reporter exclude the possibility that rhythms in grafted roots are due to leakage for the adjacent well containing the shoot. The fact that ELF4 protein shows similar properties in terms of length, molecular weight and isoelectric point to other mobile proteins[56–59] also support the notion of ELF4 movement. We postulate that following movement, the complex regulatory feedback loops at the core of the oscillator will be reset to control the pace of the clock. Further experiments at different developmental stages and various growing conditions (e.g. light and temperature) will be required to

confirm whether the long distance movement of ELF4 contributes or not to the spatial waves of clock gene expression observed in roots[42].

Excision blocks ELF4 movement from shoots and consequently, we observe that oscillator gene expression and other output genes are affected in WT excised roots. Previous studies have also used excision to define properties of the circadian function in roots[42]. Although many genes are affected by excision, it is noteworthy that 67% of the genes mis-regulated in *elf4–1* intact roots are also mis-expressed in WT excised roots. Both conditions share the lack of ELF4 movement, which suggest that the overlapped DEGs are due to the lack of a mobile ELF4 (note that the RNA-Seq studies with *elf4–1* mutant were performed with intact roots). The phase shifts observed following excision prompted us to examine whether ELF4 movement contributed to the photoperiodic-dependent phase shift. However, excised roots still sustained the phase delay under LgD suggesting that other factors are responsible for this regulation. Light piping down the root[49] might be also important for synchronization. Regardless the mechanism, it is able to overcome the mis-expression of ELF4 in shoots and roots as ELF4-ox and *elf4–1* mutant plants displayed similar rhythms to WT. Clear alteration of circadian expression under LL but not under entraining conditions has been reported for other clock mutants and over-expressing plants[60].

The EC activity is down-regulated at high temperatures in whole seedlings[29, 31]. Shoot excision shortened the period, suggesting that ELF4 movement is important in the control of circadian period length. Period shortening is more significant at low than at high temperatures confirming that ELF4 movement might be favored at low temperatures. The temperature-dependent control of ELF4 movement is also supported by the increased accumulation ELF4 protein in grafted roots at 12°C compared to 28°C. As ELF4 accumulation results in long period, the increased movement leads to a clock that runs slower at low than at high temperatures. It would be interesting to elucidate whether period sensitivity to temperature might provide an advantage for optimal root responsiveness to temperature variations.

Methods

Plant material, growth conditions, constructs and physiological assays

Arabidopsis thaliana seedlings were stratified at 4°C in the dark for 2–3 days on Murashige and Skoog (MS) agar medium with 3% of sucrose (MS3). Plates were transferred to chambers with light- and temperature-controlled conditions with 25–50 μmol·quanta·m^{-2}·s^{-1} of cool white fluorescent light. Seedlings were synchronized under Light:Dark cycles, LD (12h light: 12h dark) at 22°C. For experiments with different temperatures, seedlings were analyzed under constant light conditions at 12°C, 18°C, 22°C or 28°C following synchronization under LD (12h light: 12h dark) at 22°C. For experiments with different photoperiods, seedlings were grown under short days (ShD, 8h light: 16h dark) or long days (LgD, 16h light: 8h dark). Reporter lines *CCA1::LUC*[61], *LHY::LUC*[19], *PRR9::LUC*[62], *TOC1::LUC*[6] and *elf4–1*[17], *elf4–2*[27], ELF4 Minigene[20] and ELF4-GFP-ox[19, 20] plants were described elsewhere. The ELF4 construct fused to three Green Fluorescent Proteins (GFPs) in tandem was generated by PCR-mediated amplification of the *ELF4* coding sequence and subsequent subcloning into the PGWB514 gateway vector[63, 64]. The resulting plasmid was

digested with PacI and SacI restriction enzymes and ligated with the 3 GFPs insert from the pBS-x3GFP vector (Addgene). The construct was transformed into *elf4–1* mutant plants. Plants were transformed using *Agrobacterium tumefaciens* (GV2260)-mediated DNA transfer[65]. For in vitro protein injection assays, the ELF4 coding sequence was subcloned into the pET MBP_1a vector (Novagen) after removing the GFP by Nco I and Xho I restriction enzyme digestion.

For lateral root analyses, WT, *elf4–1* and ELF4-ox seeds were surface-sterilized and plated onto MS medium supplemented with 0.25% w/v sucrose and 1.5% agar. The top quarter of the agar was removed and seeds pipetted evenly along this line. Plants were then grown vertically for 12 days before lateral roots were measured. Lateral roots were manually counted using a Nikon SMZ800 dissecting microscope. Statistical analysis was completed using R (version 3.6), within the R studio software package (version 1.1.4). For hypocotyl elongation measurements, WT, *elf4–1*, ELF4-GFP-ox and ELF4–3xGFP-ox seeds transformed into the *elf4–1* mutant background were stratified on MS3 medium in the dark for 4 days at 4°C, exposed to white light (40 μmol·quanta·m^{-2}·s^{-1}) for 6 h and maintained in the dark (22°C) for 18 h before transferring to chambers under Short-Day conditions (8h light:16h dark). Hypocotyl length was measured using the ImageJ software (version 1.48v) (https://imagej.nih.gov/ij/) at 7 days after stratification. Each experiment was repeated at least twice using 20–50 seedlings per genotype. Statistical analyses were performed using the GraphPad Prism software (version 5.01; GraphPad Software, Inc) using two-tailed t-tests with 95% of confidence.

In vivo luminescence assays

In vivo luminescence assays were performed as previously described[47]. Briefly, 7–15 day-old seedlings synchronized under LD cycles at 22°C were transferred to 96-well plates and released into the different conditions as specific for each experiment. Analyses were performed with a LB960 luminometer (Berthold Technologies) using the Microwin software (Version 4.41; Mikrotek Laborsysteme). The period, phase and amplitude were estimated using the Fast Fourier Transform–Non-Linear Least Squares (FFT-NLLS) suite 63[66] using the Biological Rhythms Analysis Software System (version 3.0; BRASS, http://www.amillar.org). For the simultaneous analysis of rhythms of shoots and roots from the same plant, the connection between the two adjacent wells of the 96-well plates was serrated. Seedlings were then horizontally positioned so the shoot was placed in one well and the roots in the contiguous well. For excision analyses, roots were excised from shoots and placed into the 96-well plates for luminescence analyses. Data from samples that appeared damaged or contaminated were excluded from the analysis. For analyses of grafted samples, water instead of luciferin was applied to the wells containing shoots to avoid possible leaking signals from shoots to roots as specified. At least two biological replicates were performed per experiment, with measurements taken from distinct samples grown and processed at different times. Each biological replicate included 6 to 12 independent seedlings per condition and/or genotype. Statistical analyses were performed using the GraphPad Prism software (version 5.01; GraphPad Software, Inc) using two-tailed t-tests with 95% of confidence.

Protein purification and injection analyses

E. coli cells (BL21, Dh5α) were transformed and grown in LB medium (Tryptone 10 g/L, yeast extract 5 g/L, NaCl 10 g/L pH 7.5) until OD600 values of 0.8–1.0. Isopropyl β-D-1-thiogalactopyranoside (IPTG)-mediated induction of MBP-ELF4 and MBP-GFP was performed at 28°C for 6 h. Bacteria resupended in lysis buffer (50mM Tris-HCl, pH7–8, 5% glycerol, 50mM NaCl) were lysed by sonication for 2–3 minutes (30s on, 30s off, high intensity) using a sonicator (Bioruptor, Diagnode). Recombinant proteins were purified using gravity flow columns with amylose resin (New England Biolabs). MBP cleavage was performed by incubation in cleavage buffer (50 mM Trizma-HCl, pH 8.0, 0.5 mM EDTA, and 1 mM DTT) for 2 hours at 30°C with native Tobacco Etch Virus (TEV) protease (Sigma-Aldrich). The purified recombinant proteins were concentrated using Amicon centrifugal filters following the manufacturer recommendations (Millipore). Protein yield was estimated by measuring absorbance at 595 nm using a spectrophotometer (UV-2600, SHIMADZU). Proteins were also examined by Coomassie-Brilliant Blue staining of polyacrylamide gels to confirm protein size and integrity. Purified ELF4 was injected into leaves of 10-day old *elf4–1* mutant seedlings harboring the *LHY::LUC* reporter line. Similar concentration of GFP protein was also injected as a negative control. Rhythms were subsequently examined in a LB960 luminometer (Berthold Technologies) as described above.

Time course analyses of gene expression by RT-qPCR

Seedlings were synchronized under LD cycles in MS3 medium plates for 12–14 days and subsequently transferred to LL. Shoots and roots from intact plants were taken every 4 hour over the circadian cycle. For excised roots, shoots and roots were carefully separated with a sterile razor blade and the excised roots were deposited on MS3 agar medium plates for 2 or 3 days as specified. RNA was purified using a Maxwell RSC Plant RNA kit following the manufacturer's recommendations (Promega). Single-stranded cDNA was synthesized using iScript Reverse Transcription Supermix for RT-qPCR (Bio-Rad). qPCR analyses were performed with cDNAs diluted 50-fold with nuclease-free water using Brilliant III Ultra-Fast SYBR Green qPCR Master Mix (Agilent) with a 96-well CFX96 Touch Real-Time PCR detection system (Bio-RAD CFX96 Manager version 3.1, Bio-Rad). Each sample was run in technical triplicates. The expression of *PP2AA3 (PROTEIN PHOSPHATASE 2A SUBUNIT A3*, AT1G13320) or *MON1* (*MONENSIN SENSITIVITY1*, AT2G28390)[67] was used as a control. Crossing point (Cp) calculation was used for quantification using the Absolute Quantification analysis by the 2nd Derivative Maximun method. At least two biological replicates were performed, with measurements taken from distinct samples grown and processed at different times.

RNA-Seq analyses

Roots from 14-day old intact WT, *elf4–1* mutant and excised WT plants synchronized under LD cycles in MS3 medium plates were transferred to LL conditions for 3 days. Roots were excised just before transferring to LL. Samples were collected at the fourth day under LL at circadian time 75 (CT75). Total RNA was isolated using a Maxwell RSC Plant RNA kit. RNA sequencing was performed by IGATech (Italy). About 1–2 μg of high quality RNA

(R.I.N. >7) was used for library preparation with a TruSeq Stranded mRNA Sample Prep kit' (Illumina, San Diego, CA). Poly-A mRNA was fragmented for 3 minutes at 94°C. Purification was performed with 0.8x Agencourt AMPure XP beads. Both RNA samples and final libraries were quantified using the Qubit 2.0 Fluorometer (Invitrogen, Carlsbad, CA). Quality was tested using the Agilent 2100 Bioanalyzer RNA Nano assay (Agilent technologies, Santa Clara, CA). Libraries were then processed with Illumina cBot for cluster generation on the flowcell, following the manufacturer's instructions and sequenced on paired-end mode at the multiplexing level requested on HiSeq2500 (Illumina, San Diego, CA). The CASAVA (1.8.2 version) of the Illumina pipeline was used to process raw data for both format conversion and de-multiplexing.

Sequence analysis was performed using the A.I.R. software (version 1.0) (https://transcriptomics.sequentiabiotech.com/) developed by Sequentia Biotech. Briefly, raw sequence files were first subjected to quality control analysis by using FastQC (v0.10.1) before trimming and removal of adapters with BBDuk (https://jgi.doe.gov/data-and-tools/bbtools/). Reads were then mapped against the *Arabidopsis thaliana* genome (TAIR10 Genome Release, ftp://ftp.arabidopsis.org/) with STAR (version 2.6)[68]. FeatureCounts (version 1.6.1)[69] was then used to obtain raw expression counts for each annotated gene. The differential expression analysis was conducted with edgeR (version 3.18.1)[70], using the TMM normalization method. FPKM were obtained with edgeR.

The Integrative Genomics Viewer (IGV, version 2.4.13) (https://software.broadinstitute.org/software/igv/) was used to visualize the data[71, 72]. The circadian phases were analyzed using the publicly available Gene Phase Analysis Tool "PHASER" of the DIURNAL database (http://diurnal.mocklerlab.org/)[73, 74]. Phase over-representation is calculated as the number of genes with a given phase divided by the total number of genes over the number of genes called rhythmic and divided by the total number of genes in the dataset. Functional categories of the DEG were obtained using the web tool "BIOMAPS"(VirtualPlant, version 1.3)[75], which renders over-represented and significant functional terms (Gene Ontology or MIPS) as compared to the frequency of the term in the whole genome.

Western-blot assays

Approximately 50–100 mgs of roots from plants grown under the specified photoperiodic condition were sampled every four hours over a 24-hour cycle. Samples were rapidly frozen with liquid nitrogen and grounded with stainless steel beads (Millipore) in a tissue lyser (QIAGEN, TissueLyser II). Tissue was subsequently resuspended in Protein Extraction Buffer (PEB) containing 50 mM Tris-HCl pH 7.5, 150 mM NaCl, 0.5% NP40, 1 mM EDTA, and protease inhibitors cocktail (1:100) and PMSF (1:1000). Protein extracts were centrifuged at 4 °C, measured for protein concentration using Bradford reagent (Bio-Rad) and normalized to 2 mg/ml in 4 × SDS loading buffer (250 mM Tris-HCl, pH 6.8, 8% SDS, 0.08% bromophenol blue, 40% glycerol). Samples were run on a 12% gel and analyzed by immunoblotting, fixed 30 min with 0.4% Glutaraldehyde solution (Sigma-Aldrich) and detected with an anti-HA antibody (Roche) (1:2000 dilution) and a goat anti-rat horse peroxidase conjugated secondary antibody (Sigma-Aldrich) (1:4000 dilution). For analyses of the grafted plants, roots from plants synchronized under LD cycles were subsequently

transferred to LL for 3 days at 12°C, 22°C or 28°C. Samples were collected at CT81, rapidly frozen with liquid nitrogen and grounded with stainless steel beads (Millipore) in a tissue lyser (QIAGEN, TissueLyser II). Powder extracts were subsequently resuspended in Protein Extraction Buffer (PEB) containing 50 mM Tris-HCl pH 7.5, 150 mM NaCl, 0.5% NP40, 1 mM EDTA, and protease inhibitors cocktail (1:100), PMSF (1:1000), and MG132 (100uM). Protein extracts were centrifuged at 4 °C, measured for protein concentration using Bradford reagent (Bio-Rad) and normalized to 2 μg/μl in 4 × SDS loading buffer (250 mM Tris-HCl, pH 6.8, 8% SDS, 0.08% bromophenol blue, 40% glycerol and 5 mM β-mercaptoethanol). For detection of ELF4 protein fused to GFP, samples were run on a 10% gel and was detected using an anti-GFP antibody (ab290, Abcam) (1:5000) and Goat anti-Rabbit IgG (H +L) Secondary Antibody, HRP (31460, Lot: OG188649, Thermo Fisher Scientific) (1:5000 dilution).. For detection of ELF4 protein fused to HA (ELF4 Minigene) in shoots, samples were resuspended in Protein Extraction Buffer (PEB) containing 50mM TrisHCl pH7.5, 150mM NaCl, 0.5% NP40, 1mM EDTA, protease inhibitors and proteasome inhibitor (MG132, 100uM). Protein extracts in 4× SDS loading buffer (250 mM Tris-HCl, pH 6.8, 8% SDS, 0.08% bromophenol blue, 40% glycerol, 5 mM β-mercaptoethanol) were run on a 12% gel and analyzed by immunoblotting, fixed 30 min with 0.4% Glutaraldehyde solution (Sigma-Aldrich) and detected with an Anti-HA antibody High Affinity from rat IgG1 (11867423001, Sigma-Aldrich) (1:2000) and a goat anti-rat horse peroxidase conjugated secondary antibody (A9037, Sigma-Aldrich) (1:4000). The Image Lab software (version 5.2.1; Bio-Rad) was used to image the Western-blots. Membranes were stained with a Ponceau S solution following the manufacturer recommendations (Sigma). Proteins were also run on a 10% SDS-PAGE gel and stained with Coomassie-Brilliant Blue. At least two biological replicates were performed per experiment and/or condition, with measurements taken from distinct samples grown and processed at different times.

Micrografting assays

Micrografting was performed essentially as previously described[47]. Data from unsuccessful grafted seedlings that failed to properly join together or grafts that were insufficiently clear to be successful were discarded. Approximately 100–150 grafting events were performed for every combination of grafts. The percentage of successfully micrografted plants was about 30–50 % (possibly higher but only the clearly successful grafted plants were taken into account). From the successfully grafted plants, 30–60 % showed different degrees of recovered rhythms. For in vivo luminescence assays, shoots and roots of grafted plants were simultaneously examined using the protocol described above. Water instead of luciferin was added to the wells containing shoots to exclude the possibility that recovery of rhythms in roots were due to leaking signals from shoots. As specified, some grafted shoots contained no reporter fused to luciferase.

Reconstruction of driving forces by recurrence plots

Common driving forces were estimated following a several-step procedure. Suppose that we have the number K of simultaneous time series measurements $\{s_i(t)|i = 1, 2, \ldots, K, t = 1, 2, \ldots, T\}$. First, we took time differences $\tilde{s}_i(t) = s_i(t+1) - s_i(t)\,(i = 1, 2, \ldots, K, t = 1, 2, \ldots, T-1)$ of consecutive measurements and remove trends. Second, we used delay coordinates[76, 77]

$\overrightarrow{s}_i(t) = [\tilde{s}_i(t), \tilde{s}_i(t+1), \tilde{s}_i(t+2), \tilde{s}_i(t+3), \tilde{s}_i(t+4)]$ of 5 dimensional space ($i = 1, 2, \ldots, K$, $t = 1, 2, \ldots, T-4$) to obtain a recurrence plot[78]. A recurrence plot is a two-dimensional figure proposed originally for visualizing time series data. Both axes are the same time axis. If the Euclidean distance $\left\|\overrightarrow{s}_i(t_1) - \overrightarrow{s}_i(t_2)\right\| < \varepsilon_i$, where ε_i is a threshold and $t_1, t_2 \in \{1, 2, \ldots, T-4\}$, then we plot a point at (t_1, t_2). We denote this as $R_i(t_1, t_2) = 1$. Otherwise, we do not plot a point at (t_1, t_2). We denote this state as $R_i(t_1, t_2) = 0$. We controlled the value of the threshold ε_i for each component $i \in \{1, 2, \ldots, K\}$ so that 5% points, except for the central diagonal line, have points plotted. Third, we took the union for the recurrence plots to infer the recurrence plot of the common driving force[79]. Namely we declare $R(t_1, t_2) = 1$ if we have $R_i(t_1, t_2) = 1$ for at least one of $i \in \{1, 2, \ldots, K\}$. Otherwise, we have $R(t_1, t_2) = 0$. In each of the original recurrence plots, points are plotted where the driving force and the driven system are both similar. By taking their union, we can extract pairs of times where only the driving force is similar. Fourth, we applied the assumption of continuity and supplied the points at (t,t+1) and (t+1,t) for each i[80]. Namely, we forcefully declare $R(t, t+1) = R(t+1, t) = 1$ for $t = 1, 2, \ldots, T-5$. Fifth, we applied the method described[79] to convert the recurrence plot of the common driving force into time series. Here we describe the detail for this step: (i) we construct a network where each node correspond to a time point and we connect two nodes t_1 and t_2 if $R(t_1, t_2) = 1$; (ii) we assign a distance for each edge as $1 - \frac{\#\{k = 1, 2, \ldots, T-4 \mid R(k, t_1) = 1 \quad and \quad R(k, t_2) = 1\}}{\#\{k = 1, 2, \ldots, T-4 \mid R(k, t_1) = 1 \quad or \quad R(k, t_2) = 1\}}$; (iii) we obtain the shortest distance for each pair of nodes on this graph (this process approximates the geodesic distance between two time points); (iv) we apply the multi-dimensional scaling to convert the distance matrix to a time series. Namely this fifth step works as the inverse transform of a recurrence plot and we can reproduce a rough shape for the original time series. This fifth step has two mathematical proofs[81, 82]. Lastly, we extracted the component corresponding to the largest eigenvalue. The periodicity of the reconstructed common driving force X(t) was evaluated using the autocorrelation function and 10000 random shuffle surrogates[83], for each of which the order of time points is randomly exchanged. Here, the null hypothesis was that there was no serial dependence. The autocorrelation with time difference k is the correlation coefficient between X(t) and X(t+k). Thus, it is close to 1 if X(t) and X(t+k) are similar while it is close to 0 if they are not related to each other. If there is a 24h periodicity in the driving force, the autocorrelation with 24h time difference should be a value close to 1.

Confocal imaging

For *in vivo* confocal imaging, the roots of WT and ELF4-ox (fused to GFP) grafted shoots into *elf4–1* mutants were placed on microscope slides (Sigma). Fluorescent signals were imaged with an argon laser (transmissivity: 40%; excitation: 515 nm; emission range: 530-630 nm) in a FV-1000 confocal microscope (Olympus, Tokyo, Japan) using a FV-10-ASW4.2 Viewer Manager software (Olympus) with a 40x/1.3 oil immersion objective. The image sizes were about 640 × 640 (0.497 μm/pixel) and sampling speed of 4 μs/pixel. The results are representative of at least three biological replicates for grafting and about three-four images per grafts.

List of primers.—List of primers used for expression analyses, cloning and generation of 3x GFP construct.

Name	Sequence	Experiment
REF1(PP2A_A3)_EXP_F	AAGCGGTTGTGGAGAACATGATACG	Expression analysis
REF1(PP2A_A3)_EXP_R	TGGAGAGCTTGATTTGCGAAATACCG	Expression analysis
MON1_EXP_F	AACTCTATGCAGCATTTGATCCACT	Expression analysis
MON1_EXP_R	TGATTGCATATCTTTATCGCCATC	Expression analysis
PRR7_EXP_F	AAGTAGTGATGGGAGTGGCG	Expression analysis
PRR7_EXP_R	GAGATACCGCTCGTGGACTG	Expression analysis
PRR9_EXP_F	ACCAATGAGGGGATTGCTGG	Expression analysis
PRR9_EXP_R	TGCAGCTTCTCTCTGGCTTC	Expression analysis
ELF4_EXP_F	GACAATCACCAATCGAGAAT	Expression analysis
ELF4_EXP_R	ATGTTTCCGTTGAGTTCTTG	Expression analysis
CCA1_EXP_F	TCGAAAGACGGGAAGTGGAACG	Expression analysis
CCA1_EXP_R	GTCGATCTTCATTGGCCATCTCAG	Expression analysis
LHY_EXP_F	AAGTCTCCGAAGAGGGTCGT	Expression analysis
LHY_EXP_R	GGCGAAAAGCTTTGAGGCAA	Expression analysis
ELF4_CLN_F	CACCATGAAGAGGAACGGCGA	Cloning
ELF4_CLN_R	AGCTCTAGTTCCGGCAGCACCA	Cloning
MBP-ELF4_CLN_F	CATGCCATGGGCATGAAGAGGAACGGCGAG	Cloning
MBP-ELF4_CLN_R	CCGCTCGAGTTAAGCTCTAGTTCCGGCAGCAC	Cloning
PacI-pBS3xGFP-F	GGTTAATTAACGCTGGAGGATCCATGTCTA	Generation of pGWB-c3xGFP
SacI-pBS3xGFP-R	TCGAGCTCTCTAGAACTAGTGGATCTTTA	Generation of pGWB-c3xGFP

Data availability

Data and materials generated in this study are available without restriction and should be requested to Paloma Mas: paloma.mas@cragenomica.es. NGS data are deposited in NCBI with accession code PRJNA610472 (BioSample accessions SAMN14299292, SAMN14299293, SAMN14299294). Source data are provided for all figures.

Reporting Summary.—Further information on research design is available in the Nature Research Reporting Summary linked to this article.

Extended Data

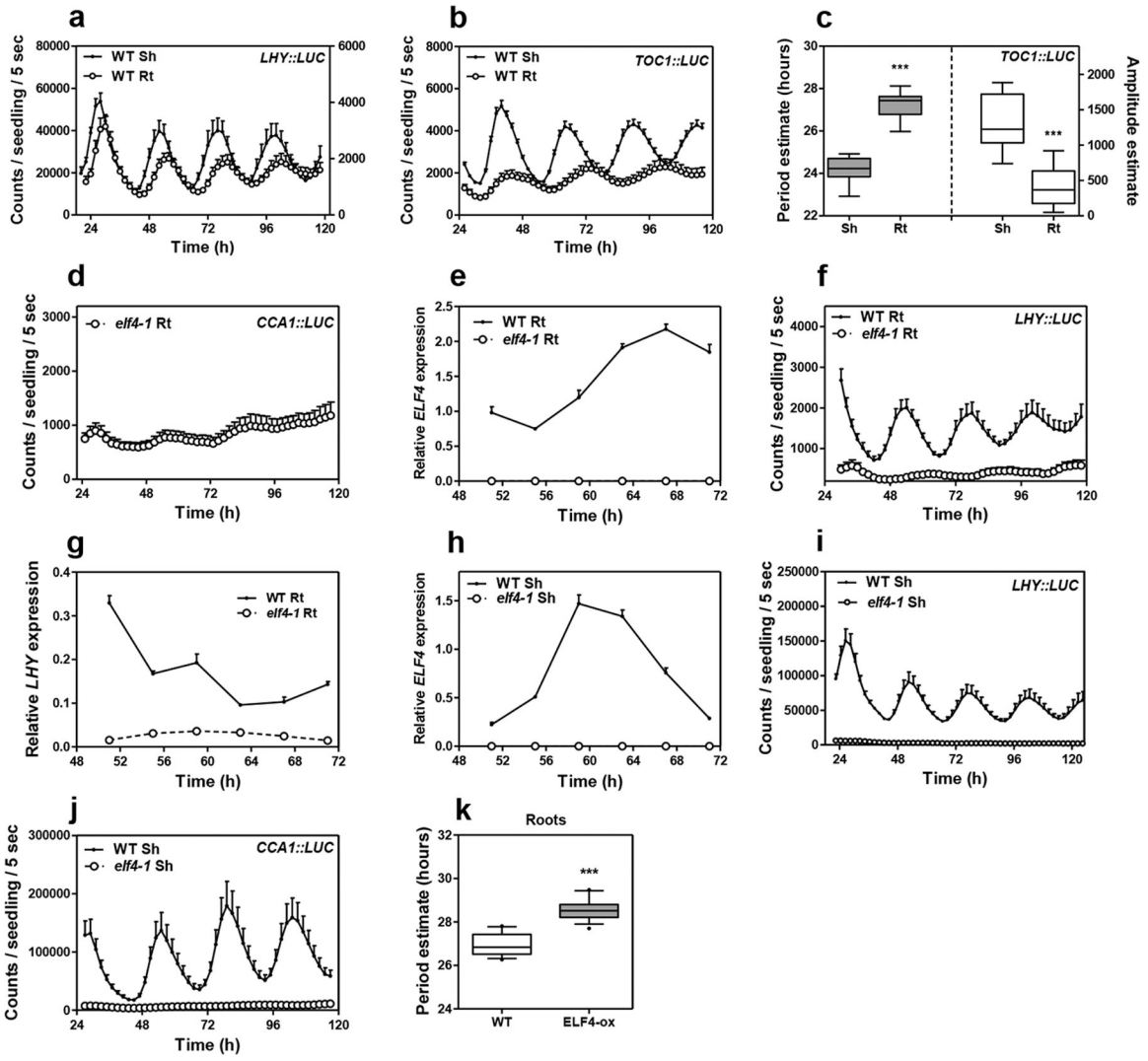

Extended Data Fig. 1. Comparative analyses of rhythmic circadian oscillation in shoots and roots.

Luminescence of **a,** *LHY::LUC* (n=6 for Sh, n=6 for Rt), and **b,** *TOC1::LUC* (n=16 for Sh, n=15 for Rt) rhythms simultaneously measured in shoots (Sh) and roots (Rt). Root luminescence signals in **a,** are represented in the right Y-axis. **c,** Circadian period (left Y-axis, n=16 for Sh, n=14 for Rt) and amplitude (right Y-axis, n=16 for Sh, n=15 for Rt) estimates of *TOC1::LUC* luminescence signals (data are represented as the median ± max and min; 25–75 percentile). *** p-value<0.0001; two-tailed t-tests with 95% of confidence. **d,** Luminescence of *CCA1::LUC* rhythms in *elf4–1* Rt (n=8) (from Fig. 1d) showing the weak rhythms of the mutant. **e,** Circadian time course analyses of *ELF4* mRNA expression in WT and *elf4–1* mutant Rt. **f,** Luminescence of *LHY::LUC* rhythms in WT (n=6) and *elf4–1* mutant Rt (n=6). **g,** Circadian time course analyses of *LHY* mRNA expression in roots of WT and *elf4–1*. **h,** Circadian time course analyses of *ELF4* mRNA expression in WT and *elf4–1* mutant Sh (also in Extended Data Fig. 3c). **i,** Luminescence of *LHY::LUC* (n=6) and **j**, *CCA1::LUC* (n=9) rhythms in WT and *elf4–1* mutant Sh. **k,** Circadian period estimates of *LHY::LUC* in WT (n=12) and ELF4-ox (n=14) roots; data are represented as the median ±

max and min; 25–75 percentile). *** p-value<0.0001; two-tailed t-tests with 95% of confidence. **a-b, d-j,** Data are represented as the means + SEM. The mRNA expression and promoter activity analyses were performed under constant light conditions previous synchronization of plants under LD cycles at 22°C. The “n” values refer to independent samples. **a-k,** Two biological replicates were performed for all experiments, with measurements taken from distinct samples grown and processed at different times.

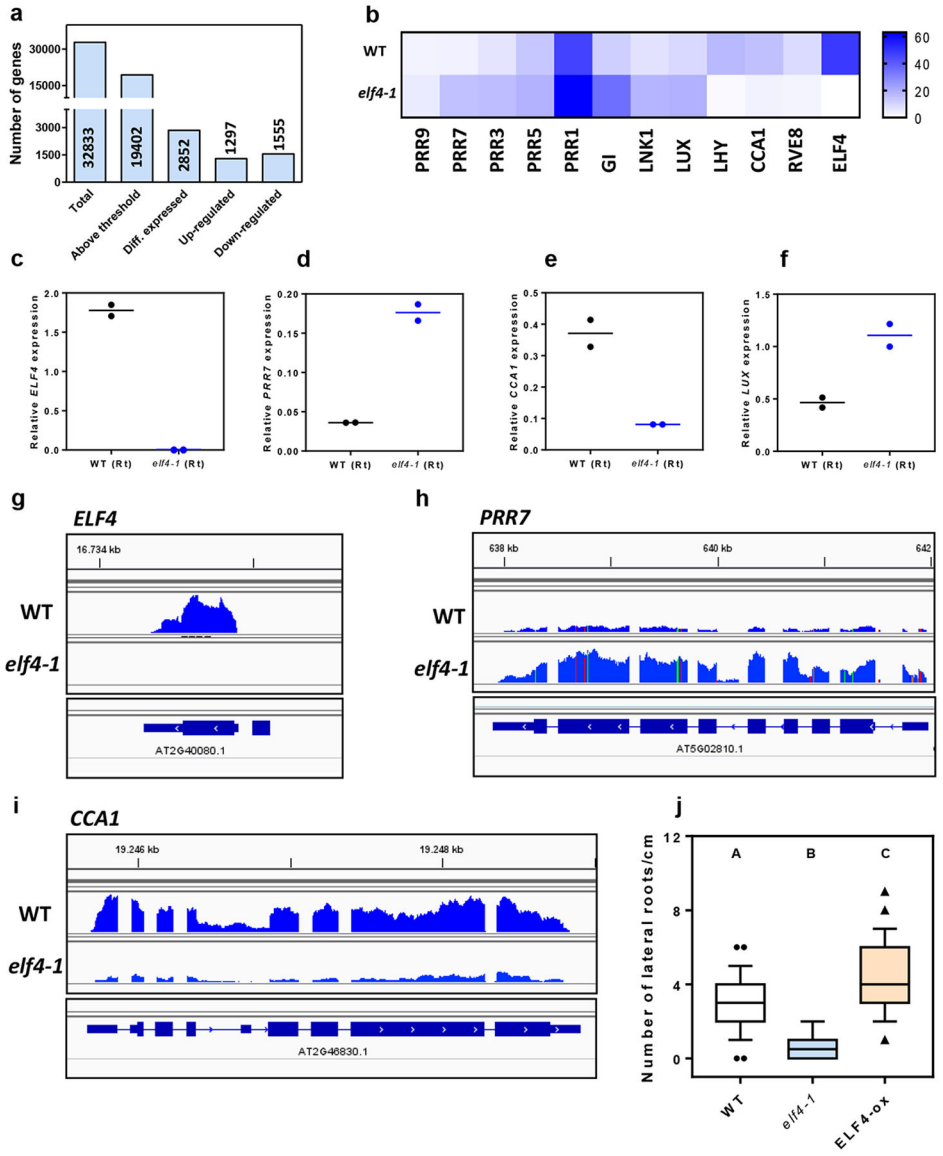

Extended Data Fig. 2. RNA-Seq analyses of WT and *elf4–1* mutant roots.

a, Quantitative analysis of DEGs in *elf4–1* versus WT roots. The statistical analyses of the DEGs are detailed in Materials and Methods. **b**, Heatmap of the median-normalized expression (Z-scaled FPKM values) of the oscillator genes in WT and *elf4–1* roots. Analyses by RT-QPCR of **c**, *ELF4*, **d**, *PRR7*, **e**, *CCA1* and **f**, *LUX* mRNA expression in roots at CT75 after three days in LL. Visualization of RNA-seq reads by using the Integrative Genomics Viewer (IGV) browser for **g**, *ELF4*, **h**, *PRR7*, **i**, and *CCA1*. **j**, Number of lateral roots per cm in the Ws-2 (WT, n=86), *elf4–1* (n=28) or ELF4-ox lines (n=48). Plants were grown for 12 days under short day (8h light:/16h darkness) photoperiod with a constant temperature of 22°C. Letters signify significant difference ($p < 0.01$) as determined by a one-way ANOVA with a Tukey HSD post hoc test. Data is represented as the median ± max and min; 25–75 percentile). Data represents an average of two independent experiments.

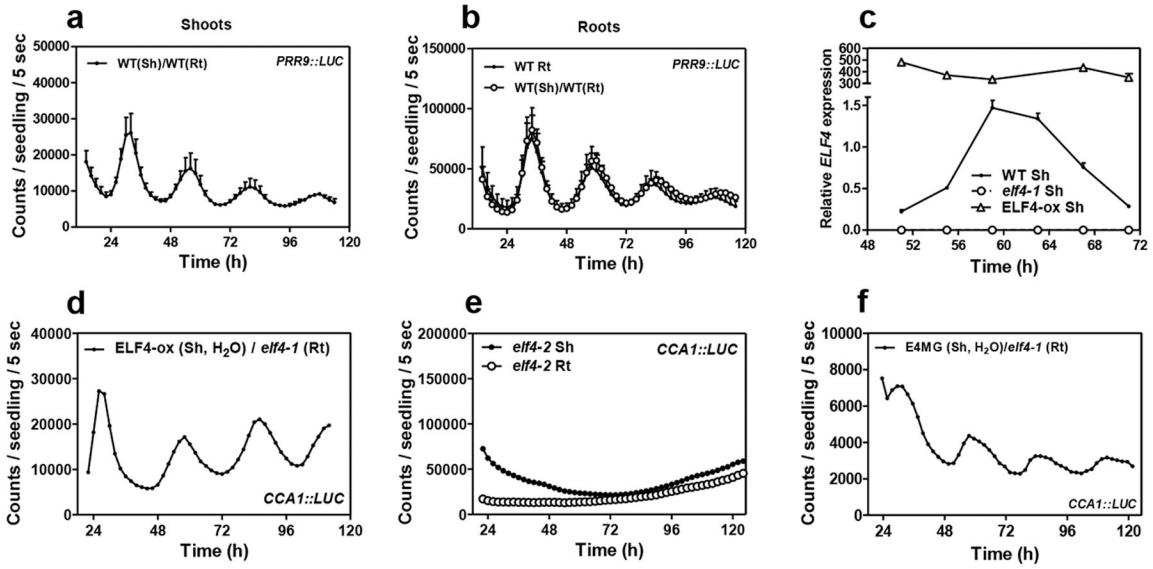

Extended Data Fig. 3. Analyses of circadian rhythmicity of the micrografting assays.

Luminescence of *PRR9::LUC* in **a,** shoots (n=3) and **b,** roots (n=3) of WT scion into WT rootstocks and its comparison with luminescence in (non-grafted) WT roots (n=4). **c,** Circadian time course analyses of *ELF4* mRNA expression in shoots of WT, *elf4–1* and ELF4-ox (also in Extended Data Fig. 1h). **d** Individual waveform of *CCA1::LUC* rhythmic recovery in roots of ELF4-ox scion and *elf4–1* rootstocks. Water instead of luciferin was added to the wells containing ELF4-ox shoots. **e,** *CCA1::LUC* luminescence in shoots and roots of *elf4–2* mutant plants (n=5 for each). **f,** Individual waveform of *CCA1::LUC* rhythmic recovery in roots of E4MG scion into *elf4–1* rootstocks. Water instead of luciferin was added to the wells containing E4MG shoots. **a-f,** Data are represented as the means + SEM. The mRNA expression and promoter activity analyses were performed under constant light conditions previous synchronization of plants under LD cycles at 22°C. The “n” values refer to independent samples. **a-f,** Two biological replicates were performed for all experiments, with measurements taken from distinct samples grown and processed at different times.

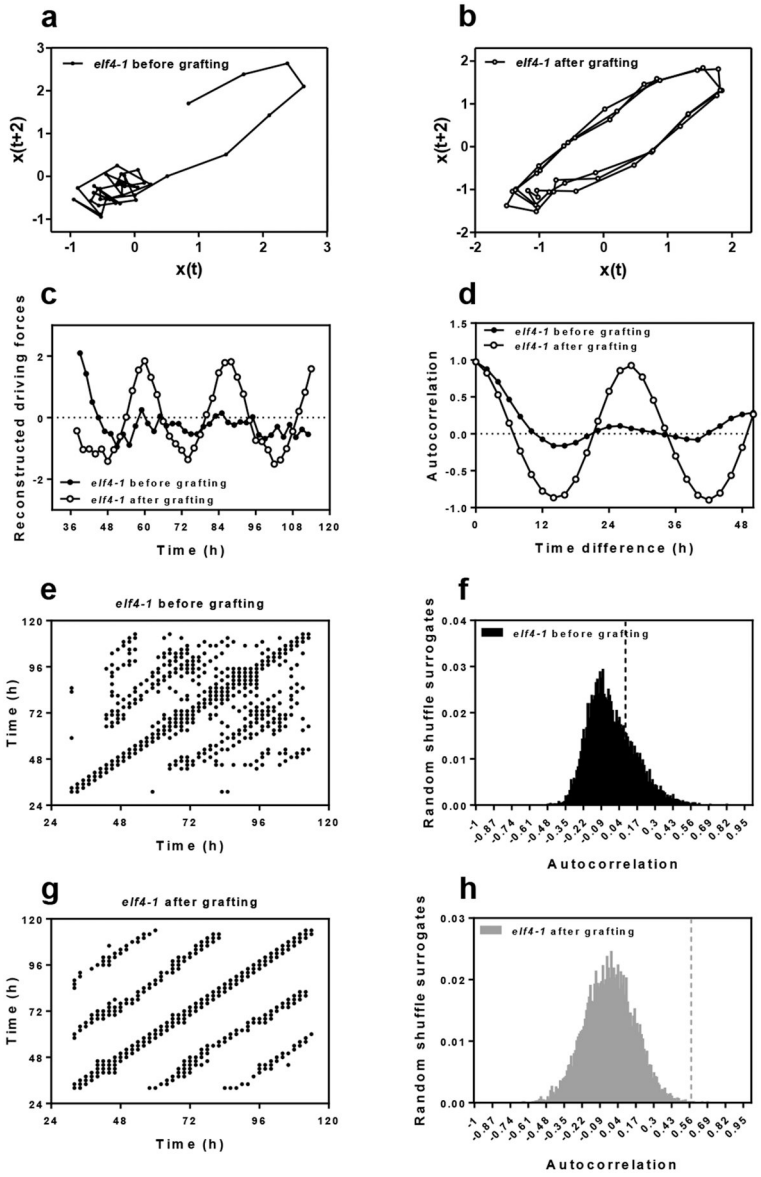

Extended Data Fig. 4. Mathematical analyses of the micrografting effects on rhythms.

Two-dimensional plots of *CCA1::LUC* rhythms in roots **a,** before and **b,** after grating ELF4-ox scion into *elf4–1* rootstocks. **c,** Reconstructed waveforms and **d,** autocorrelation analyses in roots before and after grafting. **e**, **g**, Recurrence plots for the driver obtained by delay coordinates and autocorrelation analyses **f**, before and **h**, after ELF4-ox scion grafting into *elf4–1* rootstock. Number of surrogates for each test: 10000. Before grafting: 95% confidence interval: [-1 0.2932]; effect size: 0.0975; p-value: 0.2339. After grafting: 95% confidence interval: [-1 0.2720]; effect size: 0.5752; p-value: 0.00045.

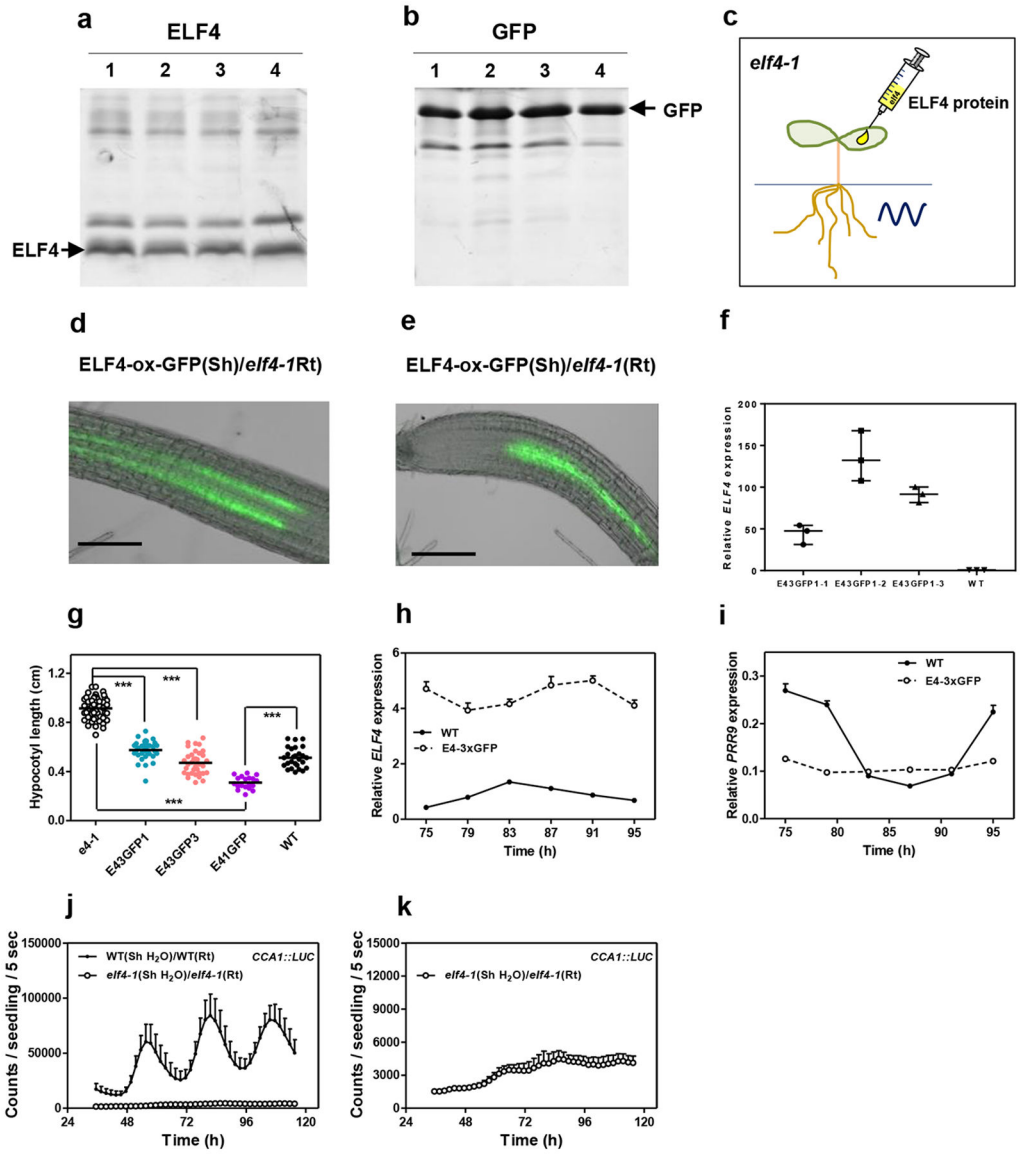

Extended Data Fig. 5. Analyses of ELF4 movement from shoots to roots.

a, ELF4 and **b,** GFP proteins purified from bacteria and **c,** injected in shoots of *elf4–1* mutant plants to examine rhythmic recovery in roots. **d, e,** Representative images showing fluorescence signals in roots of ELF4-ox-GFP scion and *elf4–1* rootstock. Scale bars: 100 μm. **f**, Gene expression analyses of *ELF4* mRNA expression in WT and different ELF4-x3GFPs lines. Data are represented as the median ± max and min; 25–75 percentile. **g,** Hypocotyl length of different lines expressing ELF4-x3GFPs (E43GFP) (E43GFP1 n=34; E43GFP3 n=35) transformed into *elf4–1* mutant plants. Hypocotyl length was also assayed for WT (n=27), *elf4–1* (n=48) and plants over-expressing ELF4 fused to 1 GFP (E41GFP) (n=19). *** p-value<0.0001; two-tailed t-tests with 95% of confidence. Data are represented as the median ± max and min; 25–75 percentile. Circadian time course analyses of **h**, *ELF4*, and **i**, *PRR9* mRNA expression by RT-QPCR in shoots of WT and ELF4-x3GFPs. **j**, Luminescence of *elf4–1* scion into *elf4–1* rootstocks *elf4–1* (Sh)/*elf4–1*(Rt) (n=4) and its

comparison with luminescence in WT (Sh)/WT(Rt) roots (n=5). **k**, Luminescence signals of *elf4–1* (Sh)/*elf4–1*(Rt) from **j**, shown in a separate graph. Water instead of luciferin was added to the wells containing WT and *elf4–1* shoots. **h-k,** Data are represented as the means + SEM. **a-k,** At least two biological replicates were performed for all experiments, with measurements taken from distinct samples grown and processed at different times.

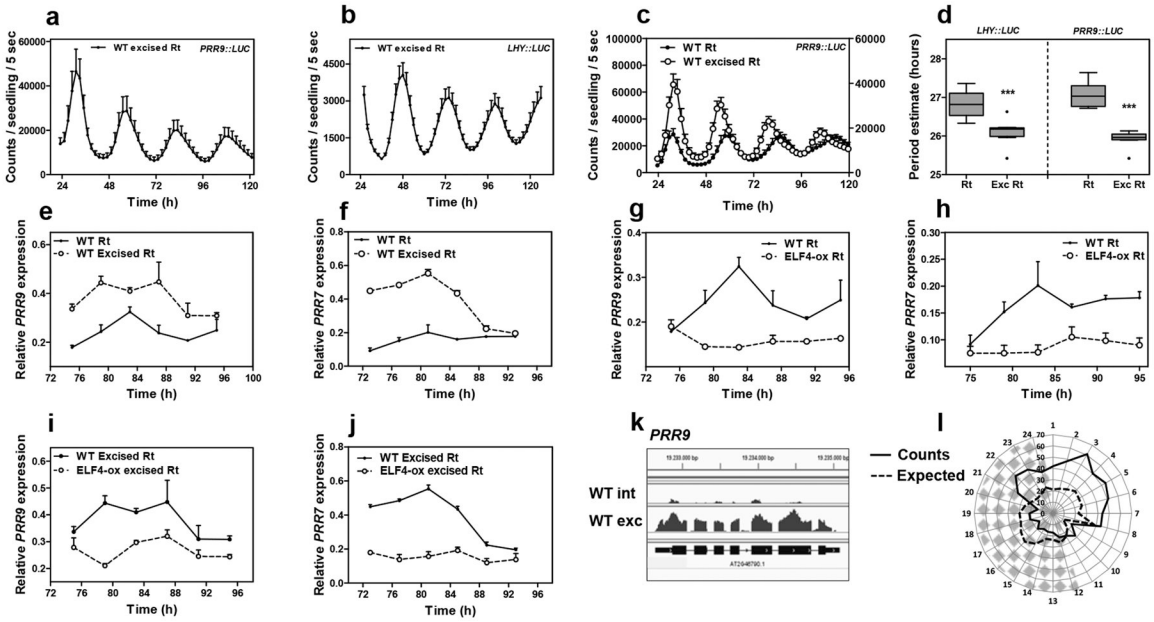

Extended Data Fig. 6. Shoot excision advances the phase and shortens the circadian period in roots.

Luminescence of **a,** *PRR9::LUC* (n=5) and **b,** *LHY::LUC* (n=8) circadian rhythms in WT excised roots. **c,** Comparison of *PRR9::LUC* circadian rhythms in WT intact (n=6) versus excised roots (n=6). **d,** Period estimates of *LHY::LUC* (left graph) (n=8) and *PRR9::LUC* (right graph) (n=8) rhythms in WT intact versus excised roots. Data are represented as the median ± max and min; 25–75 percentile. *** p-value<0.0001; two-tailed t-tests with 95% of confidence. Circadian time course analyses of **e,** *PRR9* and **f,** *PRR7* mRNA expression in WT intact versus excised roots. Circadian time course analyses of **g,** *PRR9* and **h,** *PRR7* mRNA expression in WT and ELF4-ox intact roots. Circadian time course analyses of **i,** *PRR9* and **j,** *PRR7* mRNA expression in WT excised and ELF4-ox excised roots. **a-c, e-j,** Data are represented as the means + SEM. **k,** Visualization of *PRR9* RNA-seq reads by using the Integrative Genomics Viewer (IGV) browser. **l,** Circadian phases of overlapped DEGs in *elf4–1* and WT excised roots relative to WT intact roots. Radial axis represents the subjective time (hours). White and gray areas represent subjective day and night, respectively. The mRNA expression and promoter activity analyses were performed under constant light conditions previous synchronization of plants under LD cycles at 22°C. The “n” values refer to independent samples. **a-l,** Two biological replicates were performed for all experiments, with measurements taken from distinct samples grown and processed at different times.

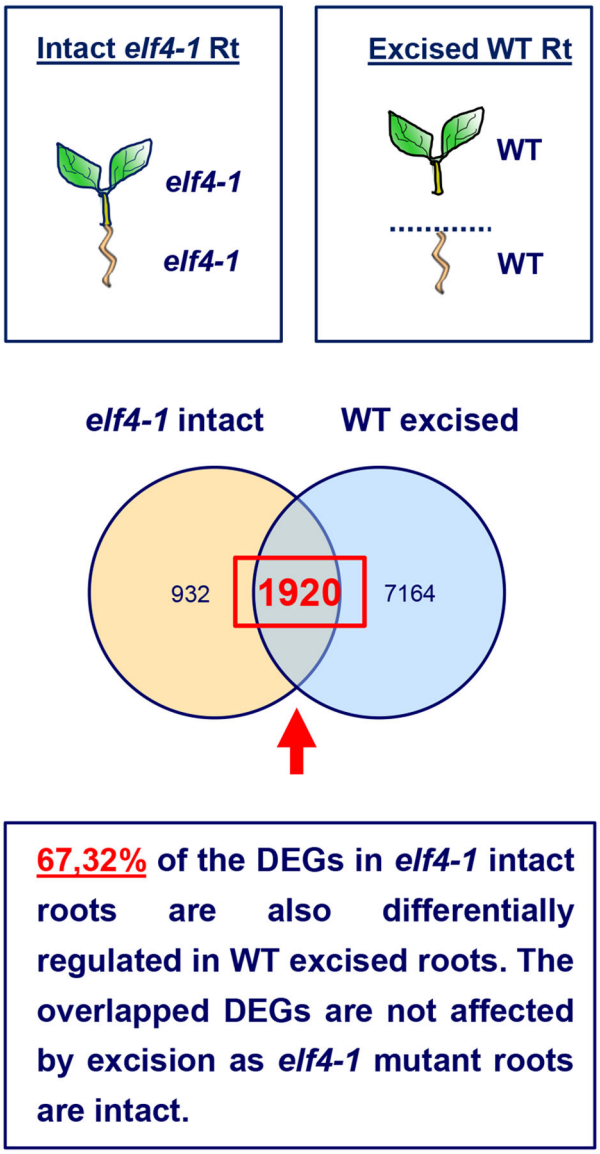

Extended Data Fig. 7. The lack of ELF4 movement affects gene expression in roots.

Schematic drawing depicting the RNA-Seq comparison of different root genotypes (*elf4–1* mutant versus WT) and conditions (intact versus excised). The proportion of overlapped DEGs (67%) is highly significant (P-value < 0.0001, chi-square test for equality of proportions) compared to the overlapped proportion of genes (30%) using random gene lists with the same counts as the DEGs in WT excised roots. The overlapped genes cannot be the result of excision because the data of *elf4–1* mutant roots come from intact roots.

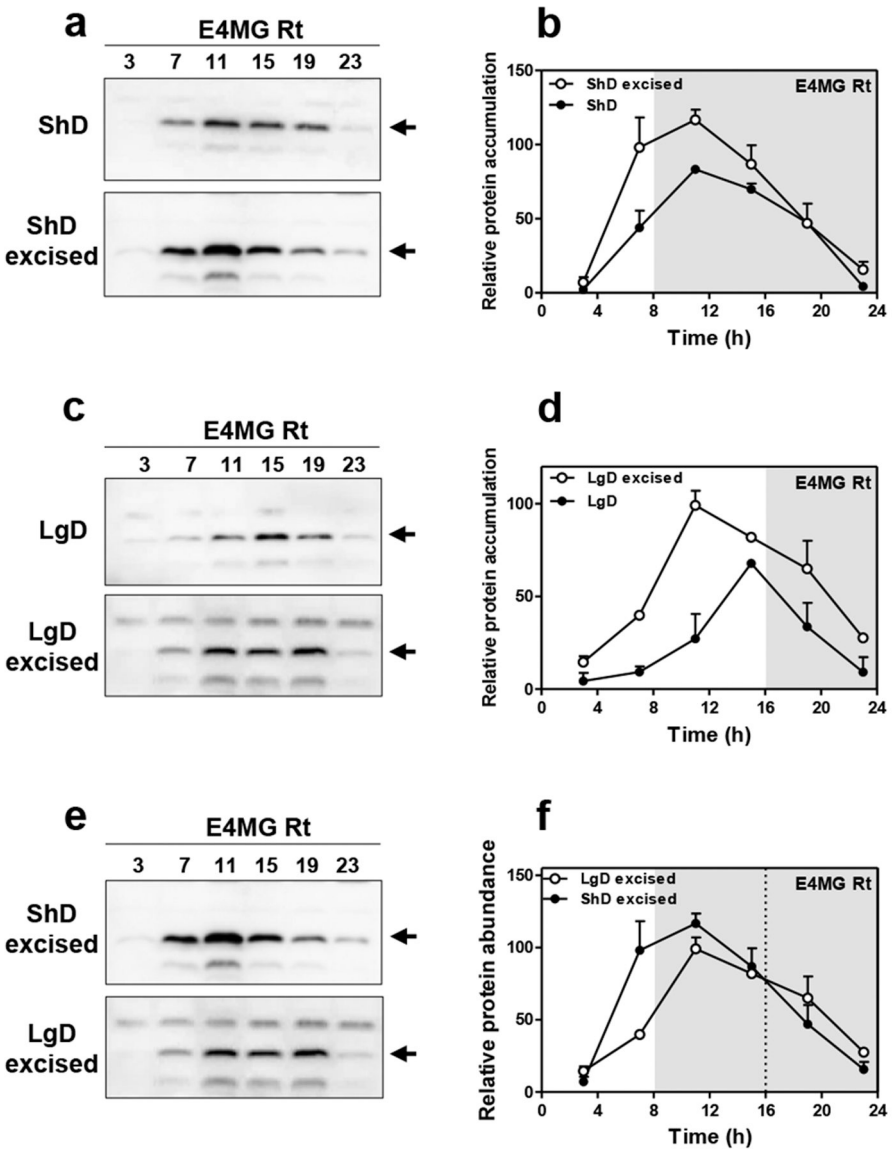

Extended Data Fig. 8. Excision advances the phase of ELF4 protein accumulation in roots under entraining conditions.

a, Western-blot analysis and **b,** quantification of ELF4 protein accumulation in ELF4 Minigene (E4MG) intact and excised roots under ShD (also in Fig. 3c–d). **c,** Western-blot analysis and **d,** quantification of ELF4 protein accumulation in E4MG intact and excised roots under LgD (also in Fig. 3e–f). **e,** Western-blot analysis and **f,** quantification of ELF4 protein accumulation in E4MG excised roots under ShD and LgD (also in Fig. 3e–f). **b, d, f,** Data are represented as the means + SEM. **a-f,** Two biological replicates were performed for all experiments, with measurements taken from distinct samples grown and processed at different times.

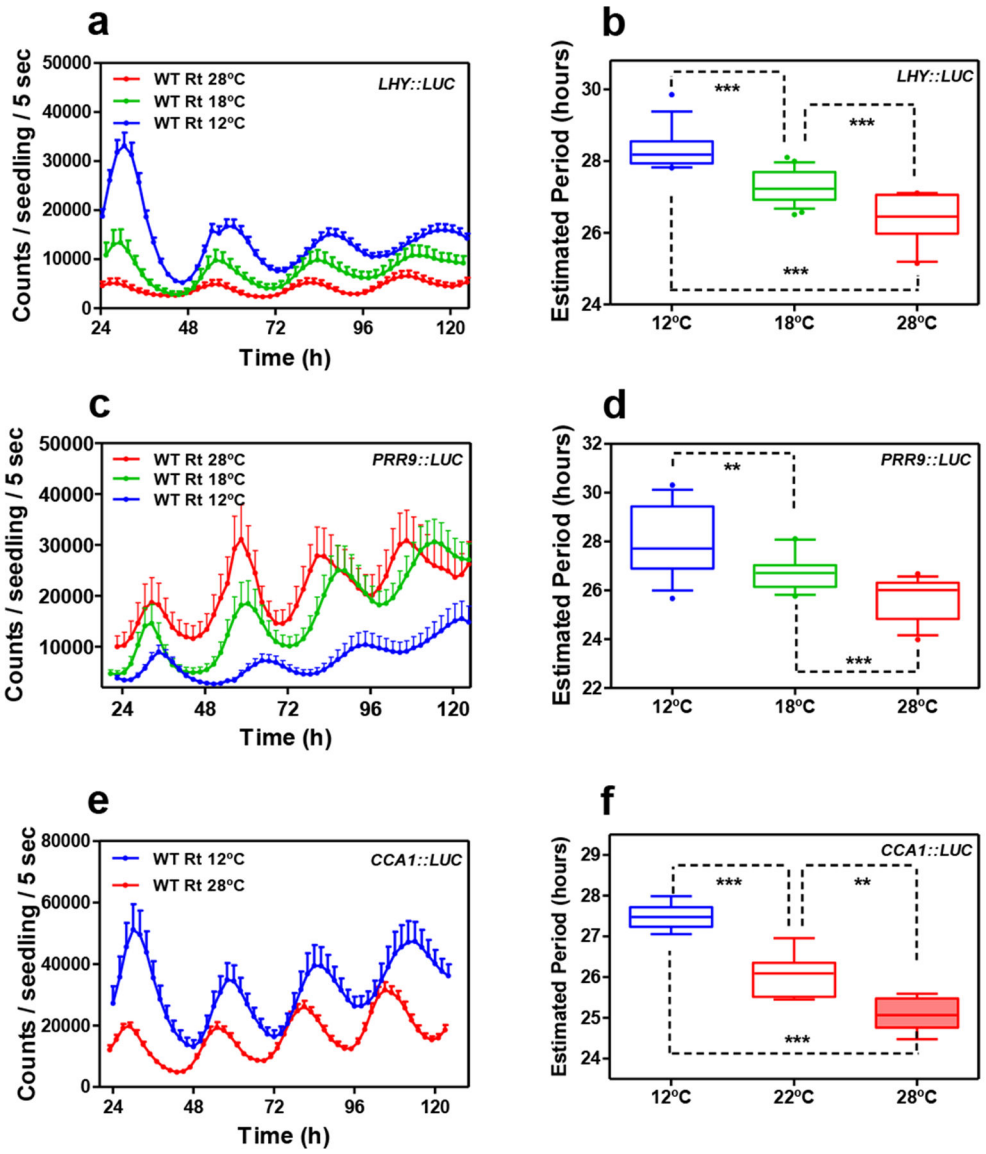

Extended Data Fig. 9. The root clock is not temperature-compensated.

a, Luminescence waveforms of *LHY::LUC* rhythmic oscillation in WT roots at 28°C (n=8), 18°C (n=8) and 12°C (n=8) and **b,** circadian period estimates of *LHY::LUC* rhythmic oscillation in WT roots at 28°C (n=12), 18°C (n=23) and 12°C (n=14). Data are represented as the median ± max and min; 25–75 percentile. **c,** Luminescence waveforms of *PRR9::LUC* rhythmic oscillation in roots at 28°C (n=8), 18°C (n=16) and 12°C (n=8) and **d**, circadian period estimates of *PRR9::LUC* rhythmic oscillation in roots at 28°C (n=14), 18°C (n=16) and 12°C (n=12). Data are represented as the median ± max and min; 25–75 percentile. **e,** Luminescence waveforms and **f**, circadian period estimates of *CCA1::LUC* rhythmic oscillation in roots at 28°C (n=6), 22°C (n=6) and 12°C (n=6) Data are represented as the median ± max and min; 25–75 percentile. **b d, f,** *** p-value<0.0001; ** p-value<0.005; *** p-value<0.0001; two-tailed t-tests with 95% of confidence. **a, c, e,** Data are represented as the means + SEM. The “n” values refer to independent samples. **a-f,** Two biological

replicates were performed for all experiments, with measurements taken from distinct samples grown and processed at different times.

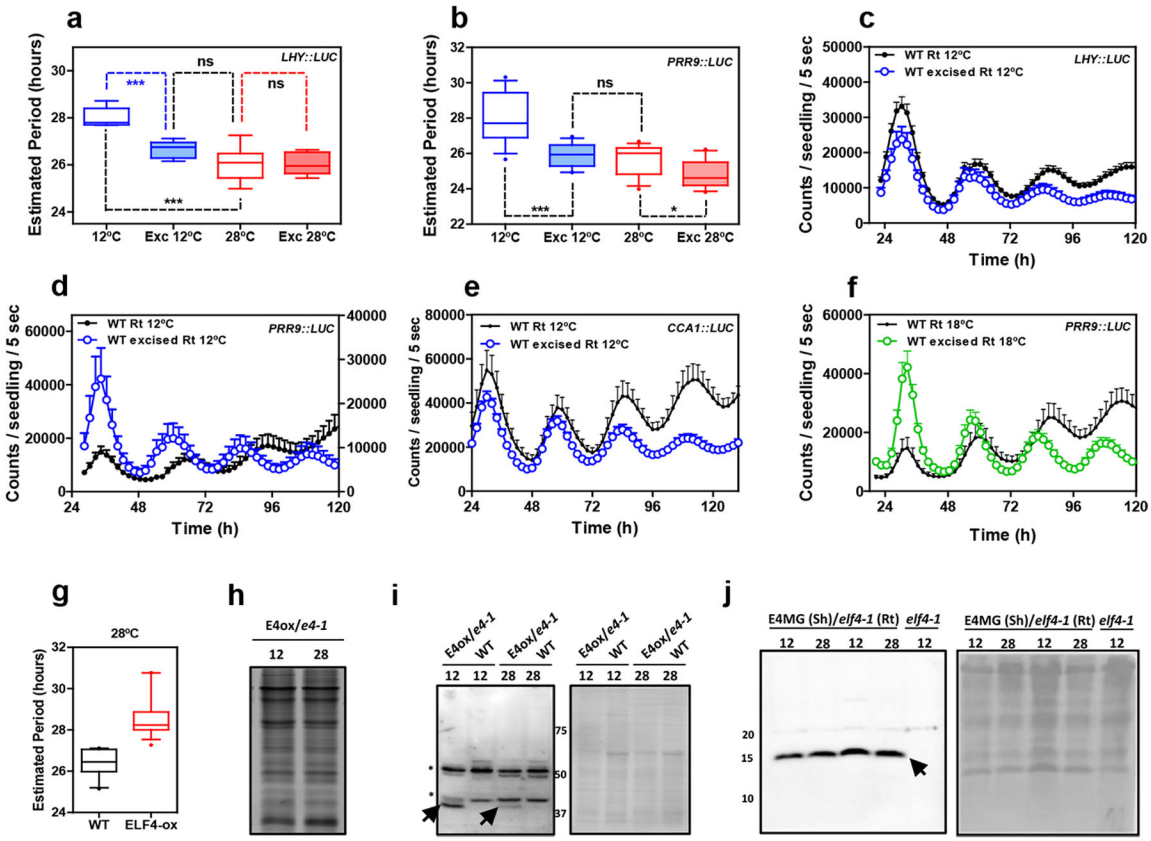

Extended Data Fig. 10. Circadian rhythms in excised roots at various temperatures.

Circadian period estimates of **a,** *LHY::LUC* in intact (n=8) versus excised WT roots (n=7) at 12°C and 28°C (n=8 for intact and n=8 for excised) and **b,** *PRR9::LUC* in intact (n=12) versus excised WT roots (n=13) at 12°C and 28°C (n=14 for intact and n=16 for excised). Data are represented as the median ± max and min; 25–75 percentile. *** p-value<0.0001; * p-value<0.05; ns: non-significant p=0.369; two-tailed t-tests with 95% of confidence. Luminescence rhythmic oscillation in WT intact and excised roots (n=8 for each) at 12°C of **c,** *LHY::LUC*, **d,** *PRR9::LUC* (n=8 for each) and **e,** *CCA1::LUC* (n=4 for excised, n=5 for intact). **f,** Luminescence of *PRR9::LUC* rhythmic oscillation in WT intact and excised roots at 18°C (n=16 for each). **c-f,** Data are represented as the means + SEM. **g,** Circadian period estimates of *LHY::LUC* in WT (n=12) and ELF4-ox (n=17) at 28°C. Data are represented as the median ± max and min; 25–75 percentile. Promoter activity analyses were performed under constant light conditions previous synchronization of plants under LD cycles at 22°C. **h,** Coomassie Blue staining of protein extracts from roots of ELF4-ox-GFP scion (E4-ox) grafted into *elf4–1* rootstock (*e4–1*) at 12°C and 28°C. **i**, Western-blot analyses of ELF4-GFP protein accumulation (arrows) in roots of ELF4-ox-GFP scion (E4-ox) grafted into *elf4–1* rootstock (*e4–1*) at 12°C and 28°C. WT protein extracts were used as a control. Asterisks denote non-specific bands. Ponceau S staining of the membrane is shown in the right panel. **j**, Western-blot analyses of ELF4 protein accumulation (arrow) in shoots of ELF4 Minigene (E4MG) grafted into *elf4–1* rootstock (*e4–1*) at 12°C and 28°C. *elf4–1* protein extracts were used as a control. Ponceau S staining of the membrane is shown in the right panel. The “n” values refer to independent samples. **a-j,** Two biological replicates were

performed for all experiments, with measurements or analyses taken from distinct samples grown and processed at different times.

Supplementary Material

Refer to Web version on PubMed Central for supplementary material.

Acknowledgments

We thank members of the Mas laboratory for helpful discussion and suggestions. We also thank Prof. T. Nakagawa (Shimane University) and Meiji Seika Kaisha, Ltd. for the Gateway vectors. We thank J. E. Salazar-Henao for tips on the Western-blot protocol in roots and Dr. I. Rubio-Somoza for sharing the GFP antibody. Research in Y.H. laboratory is supported by JSPS KAKENHI (Grant Number JP18K11461). S.J.D laboratory is funded by the Biotechnology and Biological Sciences Research Council (BB/N018540/1). S.A.K. acknowledges support from the National Institute of Health (GM067837). The Mas laboratory is funded from the FEDER/Spanish Ministry of Economy and Competitiveness, from the Ramon Areces Foundation and from the Generalitat de Catalunya (AGAUR). P.M. laboratory also acknowledges financial support from the CERCA Program/Generalitat de Catalunya and by the Spanish Ministry of Economy and Competitiveness through the “Severo Ochoa Program for Centers of Excellence in R&D” 2016–2019 (SEV-2015-0533). W.W.C. is a recipient of a CSC (Chinese Scholarship Council) fellowship.

References

1. Zhang EE & Kay SA Clocks not winding down: unravelling circadian networks. Nat. Rev. Mol. Cell. Biol 11, 764–776 (2010). [PubMed: 20966970]
2. Greenham K & McClung CR Integrating circadian dynamics with physiological processes in plants. Nat. Rev. Genet 16, 598–610 (2015). [PubMed: 26370901]
3. Nagel Dawn H. & Kay Steve A. Complexity in the wiring and regulation of plant circadian networks. Curr. Biol 22, R648–R657 (2012). [PubMed: 22917516]
4. Oakenfull RJ & Davis SJ Shining a light on the Arabidopsis circadian clock. Plant Cell Environ 40, 2571–2585 (2017). [PubMed: 28732105]
5. Hogenesch JB & Ueda HR Understanding systems-level properties: timely stories from the study of clocks. Nature Reviews Genetics 12, 407 (2011).
6. Portolés S & Más P The functional interplay between protein kinase CK2 and CCA1 transcriptional activity is essential for clock temperature compensation in Arabidopsis. PLoS Genetics 6, e1001201 (2010). [PubMed: 21079791]
7. Hansen LL, van den Burg HA & van Ooijen G Sumoylation Contributes to Timekeeping and Temperature Compensation of the Plant Circadian Clock. Journal of biological rhythms 32, 560–569 (2017). [PubMed: 29172926]
8. Marshall CM, Tartaglio V, Duarte M & Harmon FG The Arabidopsis sickle Mutant Exhibits Altered Circadian Clock Responses to Cool Temperatures and Temperature-Dependent Alternative Splicing. 28, 2560–2575 (2016).
9. Salomé P, Weigel D & McClung C The role of the Arabidopsis morning loop components CCA1, LHY, PRR7, and PRR9 in temperature compensation. Plant Cell 22, 3650–3661 (2010). [PubMed: 21098730]
10. Edwards KD, Lynn JR, Gyula P, Nagy F & Millar AJ Natural allelic variation in the temperature-compensation mechanisms of the *Arabidopsis thaliana* circadian clock. Genetics 170, 387–400 (2005). [PubMed: 15781708]
11. Edwards KD et al. FLOWERING LOCUS C mediates natural variation in the high-temperature response of the Arabidopsis circadian clock. Plant Cell 18, 639–650 (2006). [PubMed: 16473970]
12. Ito S et al. FLOWERING BHLH transcriptional activators control expression of the photoperiodic flowering regulator *CONSTANS* in Arabidopsis. 109, 3582–3587 (2012).
13. Gould PD et al. Network balance via CRY signalling controls the Arabidopsis circadian clock over ambient temperatures. 9, 650 (2013).

14. Nagel DH, Pruneda-Paz JL & Kay SA FBH1 affects warm temperature responses in the Arabidopsis circadian clock. 111, 14595–14600 (2014).
15. Jones MA, Morohashi K, Grotewold E & Harmer SL Arabidopsis JMJD5/JMJ30 Acts Independently of LUX ARRHYTHMO Within the Plant Circadian Clock to Enable Temperature Compensation. 10 (2019).
16. Gould PD et al. The molecular basis of temperature compensation in the Arabidopsis circadian clock. Plant Cell 18, 1177–1187 (2006). [PubMed: 16617099]
17. Doyle MR et al. The ELF4 gene controls circadian rhythms and flowering time in *Arabidopsis thaliana*. Nature 419, 74–77 (2002). [PubMed: 12214234]
18. Kolmos E et al. Integrating ELF4 into the circadian system through combined structural and functional studies. HFSP journal 3, 350–366 (2009). [PubMed: 20357892]
19. Herrero E et al. EARLY FLOWERING4 recruitment of EARLY FLOWERING3 in the nucleus sustains the Arabidopsis circadian clock. Plant Cell 24, 428–443 (2012). [PubMed: 22327739]
20. Nusinow DA et al. The ELF4-ELF3-LUX complex links the circadian clock to diurnal control of hypocotyl growth. Nature 475, 398–402 (2011). [PubMed: 21753751]
21. Khanna R, Kikis EA & Quail PH EARLY FLOWERING 4 functions in phytochrome B-regulated seedling de-etiolation. Plant Physiol. 133, 1530–1538 (2003). [PubMed: 14605220]
22. McWatters HG et al. ELF4 is required for oscillatory properties of the circadian clock. Plant Physiol. 144, 391–401 (2007). [PubMed: 17384164]
23. Helfer A et al. LUX ARRHYTHMO encodes a nighttime repressor of circadian gene expression in the Arabidopsis core clock. Curr. Biol 21, 126–133 (2011). [PubMed: 21236673]
24. Onai K & Ishiura M PHYTOCLOCK 1 encoding a novel GARP protein essential for the Arabidopsis circadian clock. Genes Cells 10, 963–972 (2005). [PubMed: 16164597]
25. Hazen SP et al. LUX ARRHYTHMO encodes a Myb domain protein essential for circadian rhythms. Proc. Natl. Acad. Sci. USA 102, 10387–10392 (2005). [PubMed: 16006522]
26. Hicks KA et al. Conditional circadian dysfunction of the *Arabidopsis early-flowering 3* mutant. Science 274, 790–792 (1996). [PubMed: 8864121]
27. Huang H et al. Identification of Evening Complex associated proteins in Arabidopsis by affinity purification and mass spectrometry. M. Cell. Proteomics 15, 201–217 (2016).
28. Li G et al. Coordinated transcriptional regulation underlying the circadian clock in Arabidopsis. Nat. Cell Biol 13, 616–622 (2011). [PubMed: 21499259]
29. Mizuno T et al. Ambient temperature signal feeds into the circadian clock transcriptional circuitry through the EC night-time repressor in Arabidopsis thaliana. Plant Cell Physiol 55, 958–976 (2014). [PubMed: 24500967]
30. Siddiqui H, Khan S, Rhodes BM & Devlin PF FHY3 and FAR1 act downstream of light stable phytochromes. Front Plant Sci 7, 175 (2016). [PubMed: 26941752]
31. Ezer D et al. The evening complex coordinates environmental and endogenous signals in Arabidopsis. Nat. Plants 3, 17087 (2017). [PubMed: 28650433]
32. Kim Y et al. ELF4 Regulates GIGANTEA Chromatin Access through Subnuclear Sequestration. Cell Reports 3, 671–677 (2013). [PubMed: 23523352]
33. Nieto C, López-Salmerón V, Davière J-M & Prat S ELF3-PIF4 Interaction Regulates Plant Growth Independently of the Evening Complex. Current Biology 25, 187–193 (2015). [PubMed: 25557667]
34. Sai J & Johnson CH Different circadian oscillators control Ca(2+) fluxes and lhcb gene expression. Proc. Natl. Acad. Sci. USA 96, 11659–11663 (1999). [PubMed: 10500233]
35. Thain SC, Murtas G, Lynn JR, McGrath RB & Millar AJ The circadian clock that controls gene expression in Arabidopsis is tissue specific. Plant Physiol 130, 102–110 (2002). [PubMed: 12226490]
36. Michael TP, Salome PA & McClung CR Two Arabidopsis circadian oscillators can be distinguished by differential temperature sensitivity. Proc. Natl. Acad. Sci. USA 100, 6878–6883 (2003). [PubMed: 12736379]

37. Bordage S, Sullivan S, Laird J, Millar AJ & Nimmo HG Organ specificity in the plant circadian system is explained by different light inputs to the shoot and root clocks. New Phytol 212, 136–149 (2016). [PubMed: 27240972]
38. Muranaka T & Oyama T Heterogeneity of cellular circadian clocks in intact plants and its correction under light-dark cycles. Sci. Adv 2, e1600500 (2016). [PubMed: 27453946]
39. Thain SC, Hall A & Millar AJ Functional independence of circadian clocks that regulate plant gene expression. Curr. Biol 10, 951–956 (2000). [PubMed: 10985381]
40. Fukuda H, Nakamichi N, Hisatsune M, Murase H & Mizuno T Synchronization of plant circadian oscillators with a phase delay effect of the vein network. Phys. Rev. Lett 99, 098102 (2007). [PubMed: 17931039]
41. Wenden B, Toner DLK, Hodge SK, Grima R & Millar AJ Spontaneous spatiotemporal waves of gene expression from biological clocks in the leaf. Proc. Natl. Acad. Sci 109, 6757–6762 (2012). [PubMed: 22496591]
42. Greenwood M, Domijan M, Gould PD, Hall AJW & Locke JCW Coordinated circadian timing through the integration of local inputs in Arabidopsis thaliana. PLOS Biology 17, e3000407 (2019). [PubMed: 31415556]
43. Endo M, Shimizu H, Nohales MA, Araki T & Kay SA Tissue-specific clocks in Arabidopsis show asymmetric coupling. Nature 515, 419–422 (2014). [PubMed: 25363766]
44. Yakir E et al. Cell autonomous and cell-type specific circadian rhythms in Arabidopsis. Plant J 68 520–531 (2011). [PubMed: 21781194]
45. Gould PD et al. Coordination of robust single cell rhythms in the Arabidopsis circadian clock via spatial waves of gene expression. eLife 7, e31700 (2018). [PubMed: 29697372]
46. Fukuda H, Ukai K & Oyama T Self-arrangement of cellular circadian rhythms through phase-resetting in plant roots. Phys. Rev. E 86, 041917 (2012).
47. Takahashi N, Hirata Y, Aihara K & Mas P A hierarchical multi-oscillator network orchestrates the Arabidopsis circadian system. Cell 163, 148–159 (2015). [PubMed: 26406375]
48. James AB et al. The circadian clock in Arabidopsis roots is a simplified slave version of the clock in shoots. Science 322, 1832–1835 (2008). [PubMed: 19095940]
49. Nimmo HG Entrainment of Arabidopsis roots to the light:dark cycle by light piping. Plant Cell Environ 41, 1742–1748 (2018). [PubMed: 29314066]
50. de Montaigu A, Tóth R & Coupland G Plant development goes like clockwork. Trends in Genetics 26, 296–306 (2010). [PubMed: 20483501]
51. Kolmos E et al. A Reduced-Function Allele Reveals That EARLY FLOWERING3 Repressive Action on the Circadian Clock Is Modulated by Phytochrome Signals in Arabidopsis. The Plant Cell (2011).
52. Dixon LE et al. Temporal Repression of Core Circadian Genes Is Mediated through EARLY FLOWERING 3 in Arabidopsis. Curr. Biol 21, 120–125 (2011). [PubMed: 21236675]
53. Kikis E, Khanna R & Quail P ELF4 is a phytochrome-regulated component of a negative feedback loop involving the central oscillator components CCA1 and LHY. Plant Journal 44, 300–313 (2005). [PubMed: 16212608]
54. Lu SX et al. CCA1 and ELF3 Interact in the Control of Hypocotyl Length and Flowering Time in Arabidopsis 158, 1079–1088 (2012).
55. Huang H & Nusinow DA Into the Evening: Complex Interactions in the Arabidopsis Circadian Clock. Trends in Genetics 32, 674–686 (2016). [PubMed: 27594171]
56. Corbesier L et al. FT Protein Movement Contributes to Long-Distance Signaling in Floral Induction of Arabidopsis 316, 1030–1033 (2007).
57. Jaeger KE & Wigge PA FT Protein Acts as a Long-Range Signal in Arabidopsis. Current Biology 17, 1050–1054 (2007). [PubMed: 17540569]
58. Mathieu J, Warthmann N, Küttner F & Schmid M Export of FT Protein from Phloem Companion Cells Is Sufficient for Floral Induction in Arabidopsis. Current Biology 17, 1055–1060 (2007). [PubMed: 17540570]
59. Chen X et al. Shoot-to-Root Mobile Transcription Factor HY5 Coordinates Plant Carbon and Nitrogen Acquisition. Current Biology 26, 640–646 (2016). [PubMed: 26877080]

60. Flis A et al. Defining the robust behaviour of the plant clock gene circuit with absolute RNA timeseries and open infrastructure. Open Biol 5 (2015).
61. Salomé PA & McClung CR PSEUDO-RESPONSE REGULATOR 7 and 9 are partially redundant genes essential for the temperature responsiveness of the *Arabidopsis* circadian clock. Plant Cell 17, 791–803 (2005). [PubMed: 15705949]
62. Edwards KD et al. Quantitative analysis of regulatory flexibility under changing environmental conditions. Mol. Syst. Biol 6 (2010).
63. Nakagawa T et al. Development of series of gateway binary vectors, pGWBs, for realizing efficient construction of fusion genes for plant transformation. J. Biosci. Bioeng 104, 34–41 (2007). [PubMed: 17697981]
64. Nakagawa T et al. Improved gateway binary vectors: high-performance vectors for creation of fusion constructs in transgenic analysis of plants. Biosci Biotechnol Biochem 71, 2095–2100 (2007). [PubMed: 17690442]
65. Clough SJ & Bent AF Floral dip: a simlified method for Agrobacterium-mediated transformation of Arabidopsis thaliana. Plant J 16, 735–743 (1998). [PubMed: 10069079]
66. Plautz JD et al. Quantitative analysis of Drosophila period gene transcription in living animals. J. Biol. Rhythms 12, 204–217 (1997). [PubMed: 9181432]
67. Czechowski T, Stitt M, Altmann T, Udvardi MK & Scheible W-R Genome-Wide Identification and Testing of Superior Reference Genes for Transcript Normalization in Arabidopsis. Plant physiology 139, 5–17 (2005). [PubMed: 16166256]
68. Dobin A et al. STAR: ultrafast universal RNA-seq aligner. Bioinformatics 29, 15–21 (2013). [PubMed: 23104886]
69. Liao Y, Smyth GK & Shi W featureCounts: an efficient general purpose program for assigning sequence reads to genomic features. Bioinformatics 30, 923–930 (2014). [PubMed: 24227677]
70. Robinson MD, McCarthy DJ & Smyth GK edgeR: a Bioconductor package for differential expression analysis of digital gene expression data. Bioinformatics 26, 139–140 (2010). [PubMed: 19910308]
71. Robinson JT et al. Integrative genomics viewer. Nat. Biotech 29, 24–26 (2011).
72. Thorvaldsdóttir H, Robinson JT & Mesirov JP Integrative Genomics Viewer (IGV): high-performance genomics data visualization and exploration. Brief. Bioinform 14, 178–192 (2013). [PubMed: 22517427]
73. Michael TP et al. Network discovery pipeline elucidates conserved time-of-day-specific cis-regulatory modules. PLoS Genetics 4, e14 (2008). [PubMed: 18248097]
74. Mockler T et al. The DIURNAL project: DIURNAL and circadian expression profiling, model-based pattern matching, and promoter analysis. Cold Spring Harb. Symp. Quant. Biol 72, 353–363 (2007). [PubMed: 18419293]
75. Katari MS et al. VirtualPlant: A software platform to support systems biology research. Plant Physiol 152, 500–515 (2010). [PubMed: 20007449]
76. Takens F Detecting strange attractors in turbulence. Lecture Notes in Math 898, 366–381 (1981).
77. Stark J Delay embeddings for forced systems I. Deterministic forcing. J. Nonlinear Sci 9, 255–332 (1999).
78. Marwan N, Romano CM, Thiel M & Kurths J Recurrence plots for the analysis of complex systems. Phys. Rep 438, 237–329 (2007).
79. Hirata Y, Horai S & Aihara K Reproduction of distance matrices and original time series from recurrence plots and their applications. Eur. Phys. J. Spec. Top 164, 13–22 (2008).
80. Tanio M, Hirata Y & Suzuki H Reconstruction of driving forces through recurrence plots. Phys. Lett. A 373, 2031–2040 (2009).
81. Hirata Y, Komuro M, Horai S & Aihara K Faithfulness of Recurrence Plots: A Mathematical Proof. International Journal of Bifurcation and Chaos 25, 1550168 (2015).
82. Khor A & Small M Examining k-nearest neighbour networks: Superfamily phenomena and inversion. Chaos (Woodbury, N.Y.) 26, 043101–043101 (2016).
83. Small M Applied Nonlinear Time Series Analysis: Applications in Physics, Physiology and Finance (World Scientific, 2005).

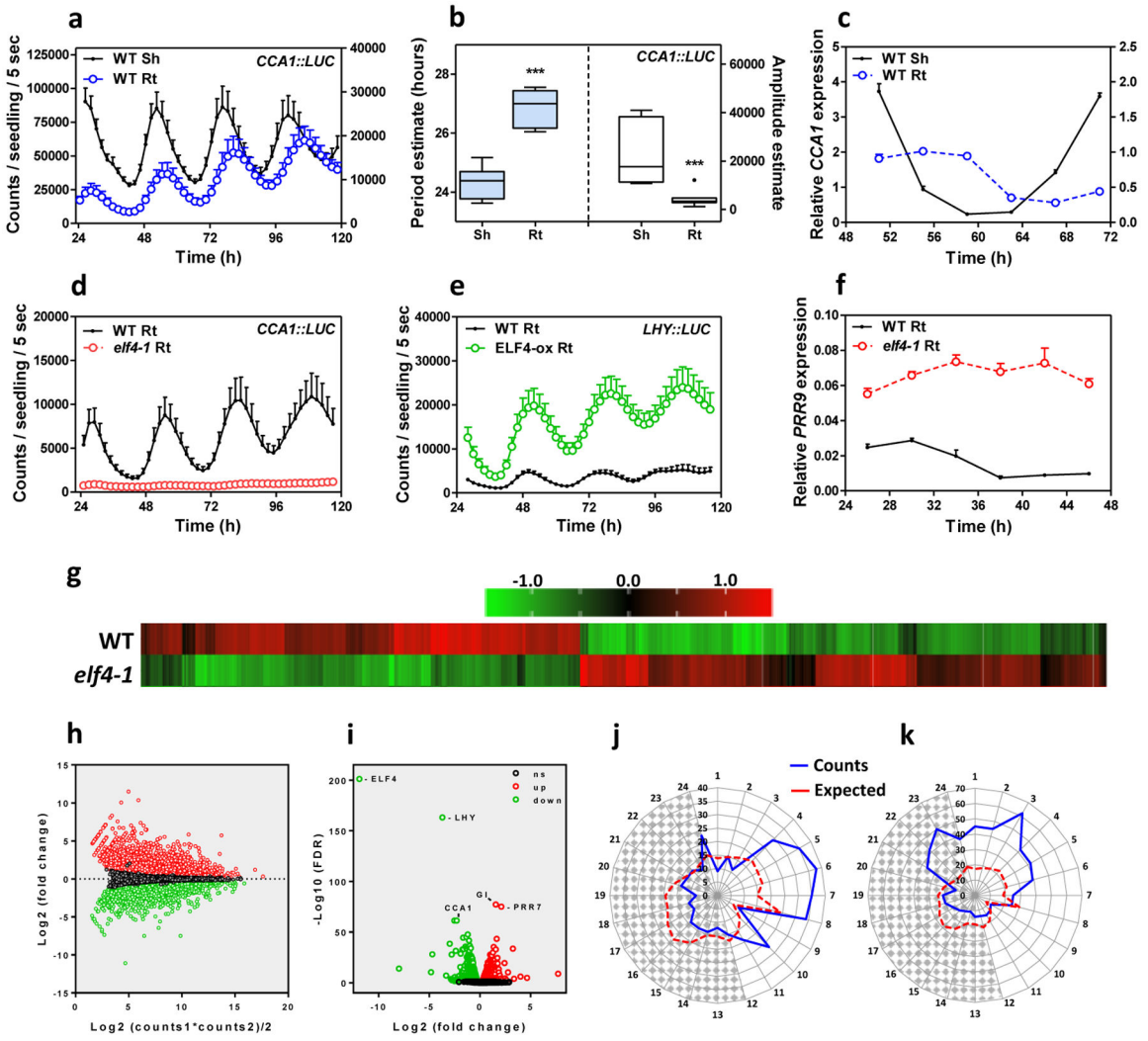

Fig. 1. Prevalent function of ELF4 sustaining circadian rhythms in roots.

a, Luminescence of *CCA1::LUC* (*LUCIFERASE*) oscillation simultaneously measured in shoots (Sh) (n=9) and roots (Rt) (n=9). Root luminescence signals are represented in the right Y-axis. **b**, Period (left Y-axis) estimates of *CCA1::LUC* rhythms in shoots and roots (n=8 for each) and amplitude (right Y-axis) estimates of *CCA1::LUC* rhythms in shoots (n=7) and roots (n=8); data are represented as the median ± max and min; 25–75 percentile). *** p-value<0.0001; two-tailed t-tests with 95% of confidence. **c**, Circadian time course analyses of *CCA1* mRNA expression in WT Sh and Rt. **d**, Luminescence of *CCA1::LUC* rhythms in WT (n=9) and *elf4–1* Rt (n=8). **e**, Luminescence of *LHY::LUC* rhythms in WT (n=8) and ELF4-ox Rt (n=9). **f**, Circadian time course analyses of *PRR9* mRNA expression in roots of WT and *elf4–1*. Sampling was performed under constant light conditions (LL) following synchronization under light:dark cycles (LD). **a, c-f**, Data are represented as the means + SEM. **g,** Heatmap of the median-normalized expression (Z-scaled FPKM values) of DEGs following a hierarchical clustering using the Euclidean distance. **h**, Relationship between average expression and fold change for each gene. **i**, Volcano plot showing fold-change versus significance of the differential expression test. Black dots represent genes that

are not differentially expressed, while red and green dots are the genes that are significantly up- and down-regulated, respectively. Circadian phases of **j**, up- and **k**, down-regulated DEG in *elf4–1* roots. Radial axis represents the subjective time (hours). White and gray areas represent subjective day and night, respectively. The “n” values refer to independent samples. **a-k,** Data for all experiments are representative of two biological replicates, with measurements taken from distinct samples grown and processed at different times.

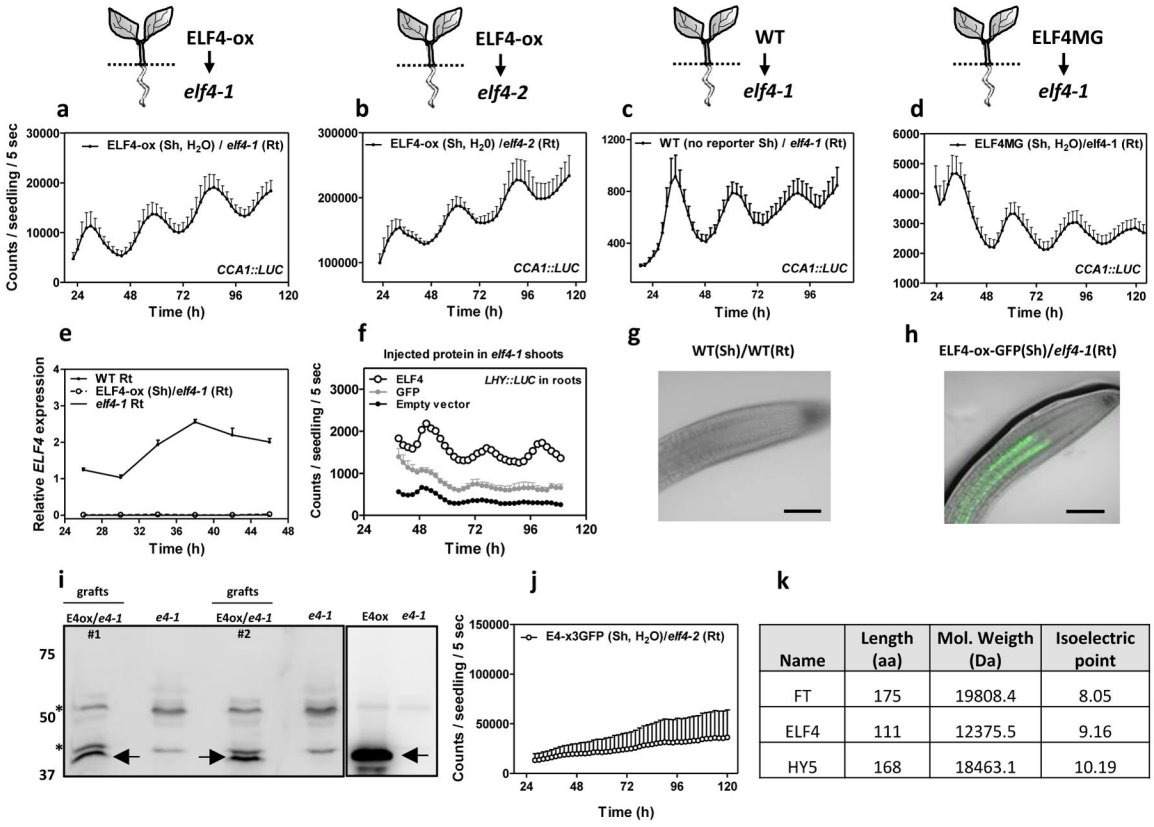

Name	Length (aa)	Mol. Weigth (Da)	Isoelectric point
FT	175	19808.4	8.05
ELF4	111	12375.5	9.16
HY5	168	18463.1	10.19

Fig. 2. ELF4 moves from shoots to regulate rhythms in roots.

CCA1::LUC luminescence in roots of ELF4-ox scion into **a**, *elf4–1* (n=4) and **b**, *elf4–2* (n=3) rootstocks. Water instead of luciferin was added to the wells containing ELF4-ox shoots. *CCA1::LUC* luminescence in *elf4–1* rootstocks with **c**, WT (n=8) and **d**, ELF4 Minigene (ELF4MG) (n=10) scions. WT scions do not express reporters and water instead of luciferin was added to the wells containing ELF4MG shoots. **a-d**, Schematic drawings depicting the different scion/rootstock combinations are shown above each graph. **e**, Circadian time course analyses of *ELF4* mRNA expression in roots of WT, *elf4–1* and ELF4-ox scion and *elf4–1* rootstocks. **f**, Luminescence of *LHY::LUC* rhythms in *elf4–1* roots after injection in shoots of purified ELF4 (n=4) or GFP proteins (n=8) and *elf4–1* roots as a control (n=6). **g,** Representative image showing the lack of fluorescence signals in roots of WT scion and WT rootstock. **h**, Representative image showing fluorescence signals in roots of ELF4-ox scion into *elf4–1* rootstock. Scale bar: 100 μm. **i**, Western-blot analysis of ELF4-GFP protein accumulation (arrows) in roots of ELF4-ox-GFP scion (E4ox) grafted into *elf4–1* rootstock (*e4–1*) (two pools of independent grafting assays, #1 and #2, are shown). Asterisks denote non-specific bands. **j,** *CCA1::LUC* luminescence in *elf4–2* rootstocks grafted with ELF4-x3GFP scions (n=5). Water instead of luciferin was added to the wells containing ELF4-x3GFP shoots. **a-f, j,** Data are represented as the means + SEM. **k**, Protein features of various plant mobile proteins. The “n” values refer to independent samples. **a-j,** Two biological replicates were performed for all experiments, with measurements taken from distinct samples grown and processed at different times.

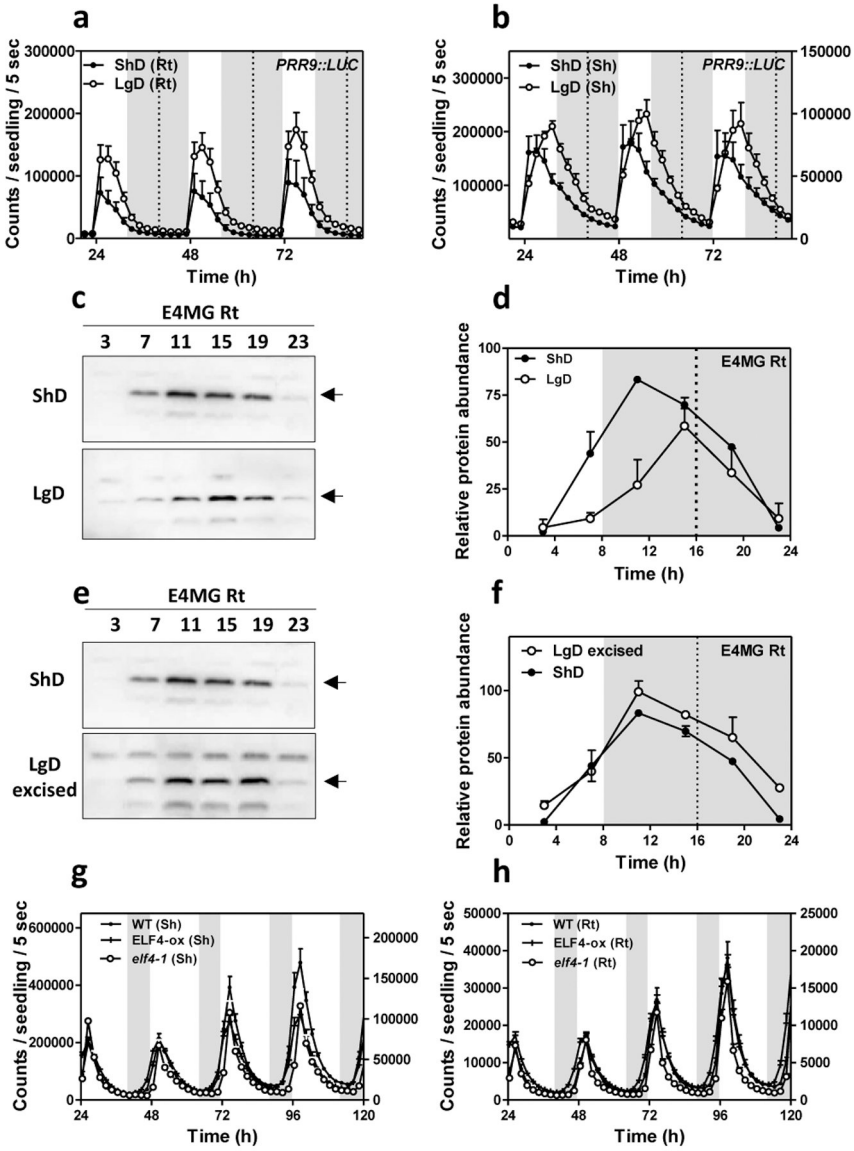

Fig. 3. Mobile ELF4 does not regulate the photoperiodic-dependent phase in roots.

Luminescence analyses of *PRR9::LUC* rhythms in **a**, roots (n=5 for ShD, n=6 for LgD) and **b**, shoots (n=6 for ShD, n=4 for LgD) of plants grown under short day (ShD) or long day (LgD) conditions. **c**, Western-blot analyses and **d**, quantification of ELF4 protein accumulation in ELF4 Minigene roots (E4MG Rt) of plants grown under ShD and LgD (also in Extended Data Fig. 8a–d). **e**, Western-blot analyses and **f**, quantification of ELF4 protein accumulation in E4MG roots of plants grown under ShD and excised roots under LgD (also in Extended Data Fig. 8a–f). Arrows indicate the ELF4 protein. Luminescence of *LHY::LUC* oscillation in WT, ELF4-ox and *elf4–1* plants measured in **g**, shoots (Sh) (n=12) and **h**, roots (Rt) (n=12) under LgD conditions. **a-b, d, f, g-h,** Data are represented as the means + SEM. Dashed lines indicate dusk under LgD. The “n” values refer to independent samples. **a-h,** Two biological replicates were performed for all experiments, with measurements taken from distinct samples grown and processed at different times.

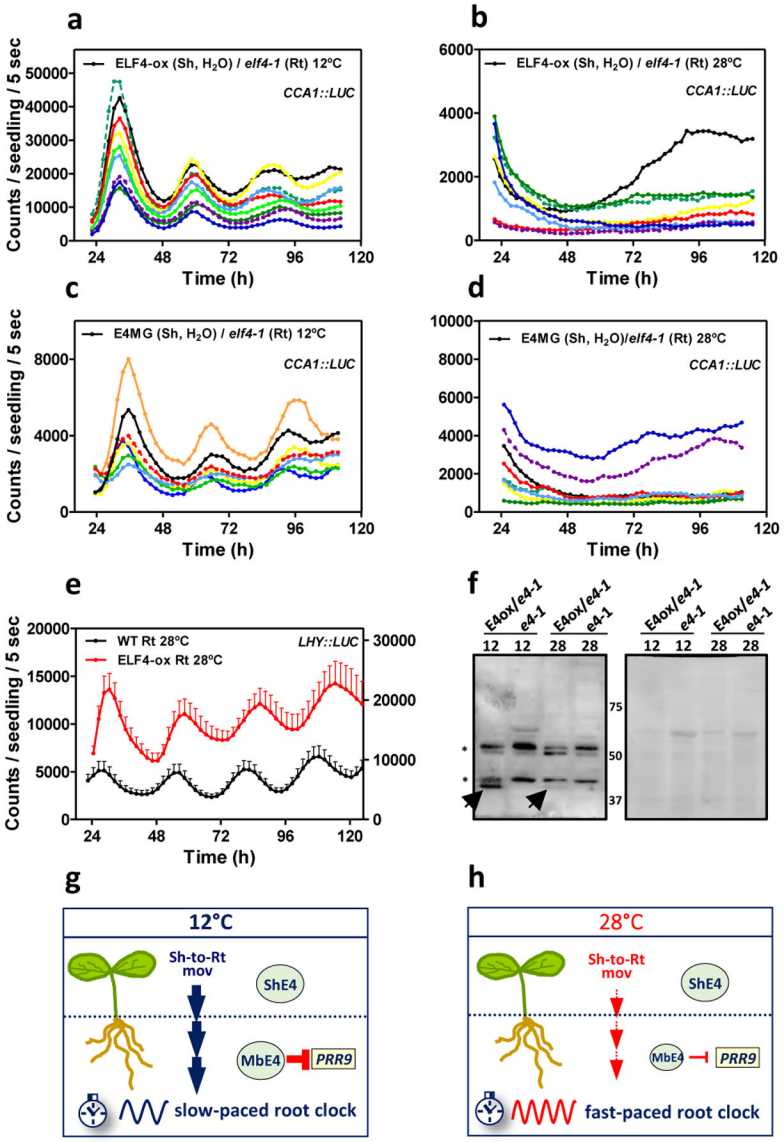

Fig. 4. Mobile ELF4 sets the temperature-dependent pace of the root clock.

Individual luminescence waveforms of *CCA1::LUC* rhythmic oscillation in ELF4-ox scion into *elf4–1* rootstocks at **a**, 12°C (n=10) and **b,** 28°C (n=8). Individual luminescence waveforms of *CCA1::LUC* rhythmic oscillation in E4MG scion into *elf4–1* rootstocks at **c**, 12°C (n=7) and **d,** 28°C (n=8).Water instead of luciferin was added to the wells containing ELF4-ox and E4MG scions. **e**, Luminescence of *LHY::LUC* rhythmic oscillation in WT and ELF4-ox roots at 28°C (n=8 for WT, n=5 for ELF4-ox). Data are represented as the means + SEM. **f**, Western-blot analysis of ELF4-GFP protein accumulation (arrow) in roots of ELF4-ox-GFP scion (E4ox) grafted into *elf4–1* rootstock (*e4–1*) at 12°C and 28°C. *elf4–1* mutant protein extracts were used as a control. Asterisks denote non-specific bands. Ponceau S staining of the membrane is shown in the right panel. Schematic drawing depicting **g**, the increased shoot-to-root movement of ELF4 (Sh-to-Rt mov, thick blue vertical arrows), increased *PRR9* repression and the slow pace of the root clock at low temperatures, and **h**,

the decreased shoot-to-root movement (Sh-to-Rt mov, thin red vertical arrows), decreased *PRR9* repression and fast-paced root clock at high temperature. The “n” values refer to independent samples. **a-f,** Two biological replicates were performed for all experiments, with measurements taken from distinct samples grown and processed at different times.